THE UNIVERSITY OF NEW SOUTH WALES

SCHOOL OF ELECTRICAL ENGINEERING AND TELECOMMUNICATION

90 Degree 1H Pulse Calibration Methods in NMR

by

Jeffrey Jiang

Thesis submitted as a requirement for the degree

Bachelor of Engineering/Master of Engineering in Electrical Engineering

Submitted: October 27, 2016

Student ID: z3463404

Supervisor: Dr. Elias Aboutanios

Course Code: ELEC4121

Co-Supervisor: Donna Lynn Kocherry

Title: 90 Degree 1H Pulse Calibration Methods in NMR

Student Name: Jeffrey Jiang   **Student ID: 3463404**

A. Problem statement

Although there is currently pulse calibration methods currently in practice, they suffer from severe inefficiency or degrading accuracy. Thus, a new method is desired to address these concerns by employing an accuracy to efficiency optimisation. The task at hand is to design or improve upon a robust algorithm for accurate 90°pulse width estimation in the nature of an NMR pulse calibration process. The algorithm is required to estimate the pulse width at the first maximum occurrence, and other parameters if necessary, of a discrete sinusoid extracted from correlated lines in an array of frequency spectra with additive Gaussian noise and quantisation noise. As an improved calibration method, the total process time should be minimised and accuracy of results optimised.

B. Objective

Review and criticise relevant literature in the field of NMR pulse calibration.
Implement accurate frequency estimation through creating and analysing a mathematical signals model. An algorithm will be chosen and refined accordingly.
Simulate the proposed calibration method using Matlab to run the algorithms and simulate test data for inspection and analysis.
With the goal of complete automation in mind, create an algorithm that is optimised for overall performance using a posteriori knowledge.

C. My solution

Spectrum peak correlation based on amplitude.
Pulse calibration using frequency estimation.
Automated process based on optimised parameters.

D. Contributions (at most one per line, most important first)

New pulse calibration method utilising digital signals processing techniques.
Optimised parameters based on both simulation and practice.
Complete automation of process.
Accuracy to efficiency trade-off.
New method performance assessment.
Comparison and contrast between new and current methods.

E. Suggestions for future work

Integrate process into Bruker Topspin software to run natively.
Enhance algorithm with dynamic, adaptive parameters to optimize with varying conditions.

While I may have benefited from discussion with other people, I certify that this report is entirely my own work, except where appropriately documented acknowledgements are included.

Signature: _____   Date: 26 / 10 / 2016

Pointers

4	Problem Statement
11	Objective

Theory (up to 5 most relevant ideas)

1	Background to NMR
5-10	Literature review
13-14	Spectral leakage
19-22	Spectrum signal model
37	Theoretical comparison of methods

Method of solution (up to 5 most relevant points)

34	Spectrum peak correlation based on amplitude
15-17	Pulse calibration using frequency estimation
29-32	Automated process based on optimised parameters

Contributions (most important first)

12-18	New pulse calibration method utilising digital signals processing techniques.
36	Optimised parameters based on both simulation and practice.
36	Complete automation of process.
29-32	Accuracy to efficiency trade-off.
37-38	New method performance assessment.
37-40	Comparison and contrast between new and current methods.

My work

15-16, 18, 36, 40	System block diagrams/algorithms/equations solved
12	Description of assessment criteria used
33-34, 36	Description of procedure (e.g. for experiments)

Results

26-35	Succinct presentation of results
36-40	Analysis
41	Significance of results

Conclusion

42	Statement of whether the outcomes met the objectives
42	Suggestions for future research

Literature: (up to 5 most important references)

15-17	[12] S. Ye, D. L. Kocherry, and E. Aboutanios.
7-8	[16] P. S. Wu and G. Otting.
6	[9] P. A. Keifer.
1-3	[6] J. Keeler.
27	[21] Y.-X. Yao and S. M. Pandit.

Abstract

In this thesis report, a novel method for determining the 90° pulse width for calibration in Nuclear Magnetic Resonance spectroscopy experiments is conceptualised and proposed. This method will aim to estimate the frequency of a real sinusoid with additive white Gaussian noise and spin physics alterations using a novel algorithm for the estimation of the parameters of a real sinusoid in noise given by Aboutanios, Kocherry and Ye. Research into current calibration methods and the potentiality of the proposed solution are presented to indicate the possible improvements in the accuracy and efficiency of the 90° pulse width determination. Simulation results are shown to prove the proposed method could provide more accurate calibration whilst also optimising the accuracy to efficiency trade-off.

Special Thanks to

Abbreviations

AMDS Aboutanios' Modified Dichotomous Search

A&M Aboutanios and Mulgrew

AWGN Additive White Gaussian Noise

DFT Discrete Fourier Transform

EMR Electromagnetic Radiation

FIM Fisher Information Matrix

FT Fourier Transform

FFT Fast Fourier Transform

NMR Nuclear Magnetic Resonance

pw90 90 Degree Pulse Width

SNR Signal to Noise Ratio

UNSW University of New South Wales

Contents

Chapter 1

Introduction

1.1 Background

Nuclear Magnetic Resonance (NMR) spectroscopy is a very powerful tool in the goal of analysing and identifying the properties of specific chemical compounds, such as structure, purity and bonds. It is a branch of spectroscopy that primarily deals with the phenomenon in which a large number of nuclei of atoms that possess magnetic moments are subjected to an external magnetic field. NMR utilises a fundamental quantum mechanical property known as spin [1]. Specifically, for the area of study of this thesis, we will be focusing on liquid state NMR and the spin of a hydrogen nucleus: A single proton. A spinning proton is similar to a rotating mass of charge, which induces a magnetic field around it[2]. When introduced into a strong external applied magnetic field, the magnetic moment μ of the nuclei can either align with the external magnetic field or against the external magnetic field; in the opposite direction. When aligned with the external magnetic field ($s = +\frac{1}{2}$), this state is known as the 'low energy spin state', or the α state, and against the magnetic field ($s = -\frac{1}{2}$) is the 'high energy spin state', or β state[3]

Obviously, there is an energy difference between these states due to the Zeeman interaction. This difference, called the Zeeman energy, is proportional to the strength of the applied external magnetic field and the physical structure, bonding, and position of the nuclei. Given by the equation:

$$E = -\mu \cdot B_0 \tag{1.1}$$

where E is the Zeeman energy and B_0 is the strength of the external magnetic field.

This energy difference between the two spin states also corresponds to a certain frequency due to the Planck relation $E = hf$, where h is the Planck constant. The corresponding characteristic angular frequency is known as the Larmor frequency, and tends to fall within the radio frequency (RF) region of the electromagnetic spectrum[4]. Therefore, exposing an element or compound to a radiation pulse containing this frequency will allow the nuclei in the α state to absorb the corresponding energy and excite to the β state.

When the RF radiation stops being applied and the excess energy is gone, those excited nuclei will fall back down to the α state. In doing so, they will emit the energy at their resonant frequency which is then detected by the NMR spectroscopic machine. This data presents itself as a Free Induction Decay (FID) signal which is composed of a superposition of exponentially decaying sinusoids, one for each of the resonant frequencies detected. In FT-NMR[5], the technique studied in this thesis, the Fourier transform (FT) of the FID signal is taken, producing a spectrum of line shapes of a characteristic Lorentzian nature, known as the chemical shift seen in Figure 1.1 below. The properties of these lines give us valuable information towards the properties of the nuclei or compound[6].
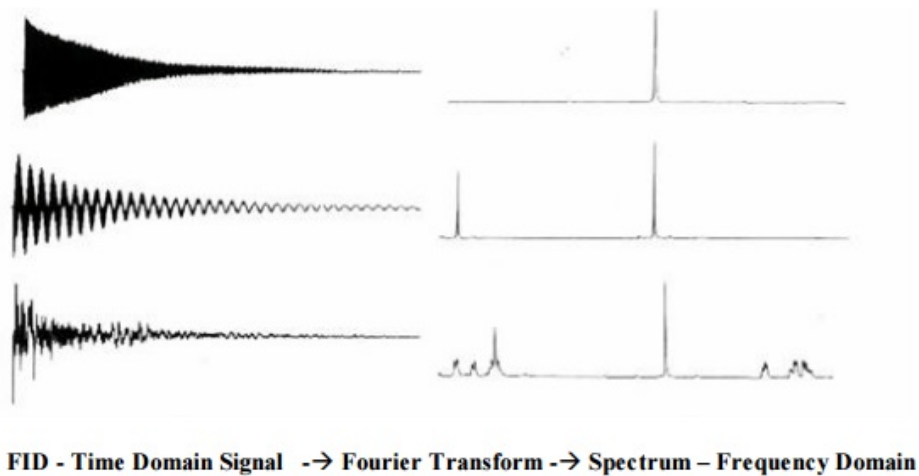

FID - Time Domain Signal -→ Fourier Transform -→ Spectrum – Frequency Domain

Figure 1.1: FIDs and Chemical Shifts[7]

1.2 Context

In the field of NMR spectroscopy, experiments rely on the radiation pulse sequence, namely the 90° pulse width (pw90)[8]. The pulses are generally defined by their angle of rotation, known as the flip angle or nutation angle, and the amount of rotation is dependent on the power and width of the pulse. A maximum signal is obtained with a 90° pulse. Thus, the pw90 is the amount of time in microseconds that the pulse of energy must be applied to the particular sample in order to produce a maximum signal to noise ratio (SNR). The value of the pw90 depends on a variety of factors including the nucleus, probe tuning and salt concentration, and can be unique even to different experiments conducted under the same conditions[9]. As such, these pulses must be calibrated as per experiment to ensure correct and optimal results.

The accurate detection of the pw90 is especially important in higher complexity NMR experiments such as correlation spectroscopy (COSY) and nuclear Overhauser effect spectroscopy (NOESY) experiments[6]. In simple routine one-pulse experiments, the pw90 can be roughly estimated without sufficiently reliable results. However, in advanced one dimensional (1D), two dimensional (2D) and higher NMR experiments, the reliance on an accurately determined pw90 is much more influential. Even seemingly insignificant errors can build up to devastating effects due to the repetitive pulsing nature of these experiments. With each repeated pulse, the error in an inaccurate pw90 value can accumulate and be the difference between an ideal spectrum and a meaningless result[10].

In this paper, we will be looking at determining the pw90 through calibration of the pulse width as the pulse power is dependent and limited to the specification of the probes being used. The ideal amplitude to pulse width relationship follows the form of a real sinusoid[9], thus the development of a robust algorithm to estimate the frequency and, hence, the pw90 is a fundamental and overlooked problem in NMR spectroscopy. Existing methods for pulse calibration do not harness the potential of signals processing and consequently suffer in both accuracy and efficiency. These methods are unacceptably outdated or incompetent in accurate estimation of the pw90.

An algorithm based on a digital signals processing method such as Aboutanios and Mulgrew's (A&M)[11] and Aboutanios, Kocherry and Ye's[12] frequency estimation algorithm could see to a great improvement in both increasing the efficiency and accuracy of the calibration process and, therefore, in the experiment of interest to follow.

1.3 Problem Statement

Although there is currently pulse calibration methods currently in practice, they suffer from severe inefficiency or degrading accuracy. Thus, a new method is desired to address these concerns by employing an accuracy to efficiency optimisation. The task at hand is to design or improve upon a robust algorithm for accurate 90° pulse width estimation in the nature of an NMR pulse calibration process. The algorithm is required to estimate the pulse width at the first maximum occurrence, and other parameters if necessary, of a discrete sinusoid extracted from correlated lines in an array of frequency spectra with additive Gaussian noise and quantisation noise. As an improved calibration method, the total process time should be minimised and accuracy of results optimised.

1.4 Outline

Throughout this thesis report, an alternative method for 90° pulse calibration in NMR experiments is constructed. The current calibration methods are assessed and a proposed alternative method is presented to improve and refine upon the current method based on parameter optimisation. The novel frequency algorithm developed by Aboutanios, Kocherry and Ye[12] will be analysed and selected as the potential enhancement. By employing the algorithm, the number of required samples and destructive spin effects can be reduced, and the efficiency and accuracy can be maximised.

In Chapter 2, a literature review for the current methods in use, consisting of Parameter Optimisation and PulseCal. Chapter 3 jumps into the proposed solution to improve on calibration processes with the new frequency estimation algorithm. Chapter 4 states the objectives of this thesis and Chapter 5 shows the preliminary signal modeling of the system. The simulated and practical results of the new calibration process are presented in Chapter 6 and 7 respectively. Chapter 8 discusses the results and provides a comparison with the current methods. Finally, Chapter 9 concludes the report with a reiteration of important points and possibilities for the future work and expansion.

Chapter 2

Literature Review

The two main calibration methods currently in use are the POPT and PulseCal pulse calibration methods.

2.1 Parameter Optimisation (POPT) Method

2.1.1 Method of Operation

This method involves the setting of an array of incrementally increasing pulse width values and subjecting the target to a series of repeated irradiation and scans with each of these pulse widths. Each of these repetitions are known as a one-pulse experiment and are calibrated with a delay-pulse-acquire sequence. The fundamental NMR equation

$$\omega_1 = \gamma \times B_1 \tag{2.1}$$

where ω_1 is the rate of rotation around the B_1 vector, referred to as the nutation, and γ is the gyromagnetic ratio of the nucleus being observed, shows us that because the nutation frequency of a nucleus is directly proportional to γ, the duration of its pw90 is inversely proportional to γ [9].

This means that each one-pulse experiment with differing pulse widths will cause the active nucleus to absorb and re-emit differing levels of energy, resulting in a unique free induction decay (FID) for each scan. The FIDs of varying amplitudes are then Fourier transformed. Doing so results in a collection of spectra that, when plotted side by side, the main peaks will represent a discrete sinusoidal envelope that is proportional to the response from the given NMR-active nucleus, as seen in Figure 2.1. Basic math is then applied to this sinusoid to find the maximum peak response, usually via finding null points at $180°$ or $360°$ and dividing by 2 or 4 respectively[13].
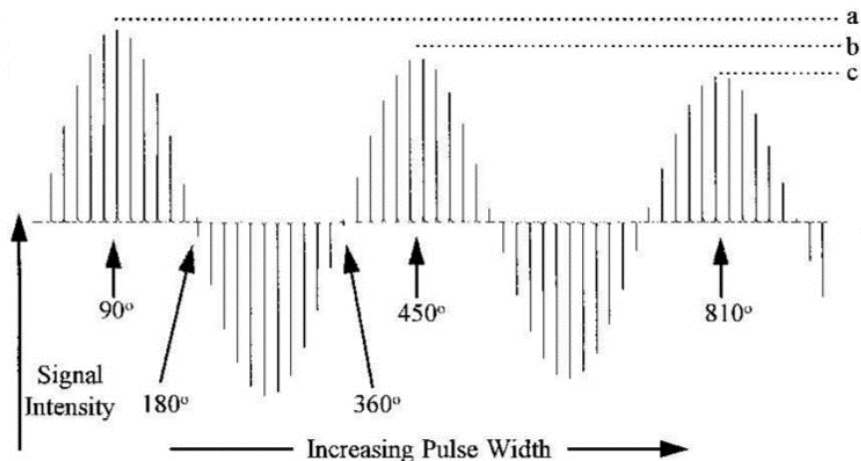
Figure 2.1: Sinusoidal nature of a POPT spectrum[9]

a, b and c all point to the peaks, however only a is considered as the pw90.

2.1.2 Disadvantages

This method is simple, however, it is practically flawed in both real world application and also in the field of signals processing. Each pulse width in the array is essentially an NMR experiment in itself. This causes a relatively large calibration time, having to wait at least the T_1 relaxation time between each one-pulse experiment[14]. This usually means that the calibration process is far longer than the actual following experiment conducted using the pw90 calibration information. Secondly, the basic math involved is greatly insufficient to conclude a calibrated pulse width. The sinusoid envelope is essentially discrete and applying continuous properties to it without prior interpolation or estimation will give large, growing errors with every consecutive step. In many cases the envelope is hardly sinusoidal at all as there are several aspects of spin physics which can alter the sinusoidal response expected during a pulse width calibration such as T_1 abuse and radiation damping[9, 15]. Assuming a perfect sine wave, as POPT does, is a crucial mistake as it will most likely be skewed and imperfect and using division of null points to estimate the peak will be far from ideal.

2.1.3 Summary

Advantages:

- Extremely simple

Disadvantages:

- Long calibration time

- Uses basic sin properties on a discrete, imperfect sinusoid which will produce errors

- May not be amenable to automation; pulse width array and peak correlation may require human input and judgment

- Affected by radiation damping, T1 abuse, and off-resonance behaviour, relaxation during pulse, etc.

2.2 PulseCal (Nutation) Method

2.2.1 Method of Operation

This method, proposed by Wu and Otting[16], for rapid pulse length determination revolves around measuring the nutation of the magnetisation vector directly instead of post-collection of a series of spectra. This method is claimed to have a much faster total calibration time as the irradiation and sampling is done 'simultaneously and continuously'. As the nucleus is subjected to continuous irradiation along the x-axis, the net magnetisation vector rotates about the z-y plane. The frequency of this nutation is directly proportional to the pulse power, hence, the nutation angle is directly proportional to the pulse width. By taking the Fourier transform of this magnetisation vector's FID, the frequency of the rotation in the z-y plane can be found. Since the projection of vector on the y-axis oscillates as a sine wave, the Fourier transform will produce an anti-phase doublet centred around zero, with the distance Δv between being double the frequency of nutation. The inverse of the frequency produces the $360°$ (one full rotation around the z-y plane) pulse width and the $90°$ pulse width would simply be a quarter of that, ie. pw90 $= \frac{1}{2\Delta v}$

Since the detection is done continuously, the time needed for calibration in the PulseCal method is far shorter than the total time of repeated experiments of the POPT method. Apart from time, the main advantage of this method is the compatibility for automation. $90°$ pulse calibration is a necessary prerequisite to any NMR experiment but does not provide useful information in itself. Therefore, automation of this repetitive process is highly requested. With the use of only one nutation scan and no user inputted variables, this method is prime for automation as every step does not require any judgement or insight, only calculation.

Wu and Otting also claim that their method is very accurate in regards to carrier frequencies that are off-resonance. Giving the effective nutation frequency $\omega_{eff} = \sqrt{\omega_1 + \Omega}$, where ω_1 is the RF carrier frequency and Ω is the difference between the RF and the Larmor frequency. Using this Pythagorean formula, at high frequencies, carrier frequencies that are significantly off-resonance still produce small errors in the effective frequency and pulse width determination.

2.2.2   Disadvantages

The main issue in this technique is that the sample must be irradiated and detected *'simultaneously'*. Of course this is not practical and instead is done by sequencing the pulse into duty cycle periods of irradiation followed by detection when the power is turned off. This technique is common to Homonuclear decoupling in which the sample is irradiated during the data acquisition by dividing each dwell time into a part for radiofrequency irradiation and a part for sampling a data point[17]. As the pulse is broken down, the rotation speed of the magnetisation vector in the z-y plane is likewise scaled down by a factor proportional to the duty cycle d for irradiation. This results in a practical nutation frequency of $f = \frac{\Delta v}{2d}$ and pulse width pw90 $= \frac{d}{2\Delta v}$ and the need for estimation of the true pw90.

Secondly, an invisible symptom that has yet to be addressed, and possibly the biggest risk of employing the PulseCal method in practice is its dependency on linear amplifiers. PulseCal method is required to be performed with reduced pulse power, known as a soft pulse, during irradiation to avoid sample heating and extreme thermal noise from the continuous radiation. In order to compensate for the lowered power, linear amplifiers must be relied upon to recreate the full powered hard pulse necessary. This is a serious problem in the accuracy over time and use, as amplifiers can degrade and inherit non-linear characteristics and clip power peaks, cause distortions and severely reduce the SNR[18].

2.2.3   Summary

Advantages:

- Highly efficient; only requires one scan

- Can be automated; no human input required

- Robust to offsets in nutation frequency

Disadvantages:

- More practically complex; irradiate and sample at the same time

- Must be performed with reduced power to avoid sample heating

- Dependent on degrading components; hard pulse must be calculated with linear amplifiers

- Performs poorly for salty solutions

2.3 Aboutanios and Mulgrew Algorithm

Previously, Aboutanios' modified dichotomous search[19] algorithm was considered for the frequency estimator of choice. However, further research has been conducted and the decision was made that the Aboutanios and Mulgrew[11] algorithm is better suited for conditions of this thesis. The A&M algorithm will be studied in this thesis and expanded upon as the focal frequency estimator. It shows promising results in estimating the frequency of a complex exponential in additive white Gaussian noise (AWGN) as, with sufficient resolution and iterations, it follows the Cramér–Rao lower bound (CRLB) very closely past its SNR threshold.

2.3.1 Method of Operation

The A&M algorithm is constituted of two stages, a coarse search using a maximum bin search (MBS) followed by a finer, focused search. The MBS stage consists of an N-point FFT of the signal and finding the maximum bin in the spectrum. The fine frequency estimator uses an interpolation search process to iteratively pinpoint the frequency of the true peak. In each iteration the two complex DFT coefficients at the bin edges are compared and used to interpolate a new maximum search bin with lower range and higher effective resolution. This process is repeated until a sufficient estimation of the frequency is obtained. The pseudocode of the algorithm is shown below in Table 2.1.

Given	A complex exponential $x(n), n = 0, \ldots, N-1$;
Find	$X(k) = \text{FFT}(x)$ and $Y(k) = |X(k)|^2$;
Find	$\hat{m} = \arg\max_k Y(k)$;
Set	$\hat{\delta} = 0$;
Loop	For i from 1 to 2, do
	$(1)\ X_{\pm} = \sum_{n=0}^{N-1} x(n)e^{-j\frac{2\pi}{N}(\hat{m}+\hat{\delta}\pm 0.5)n}$;
	$(2)\ \hat{\delta} = \hat{\delta} + \Re\{h_c\}$ or $\hat{\delta} = \hat{\delta} + \frac{N}{2\pi}\angle\hat{z}$,
	where $h_c = \frac{1}{2}\frac{X_+ + X_-}{X_+ - X_-}$, and
	$\hat{z} = \left[\cos\left(\frac{\pi}{N}\right) - 2jh_c \sin\left(\frac{\pi}{N}\right)\right]^{-1}$;
Find	$\hat{f} = \frac{\hat{m}+\hat{\delta}}{N}$.

Table 2.1: A&M pseudocode[12]
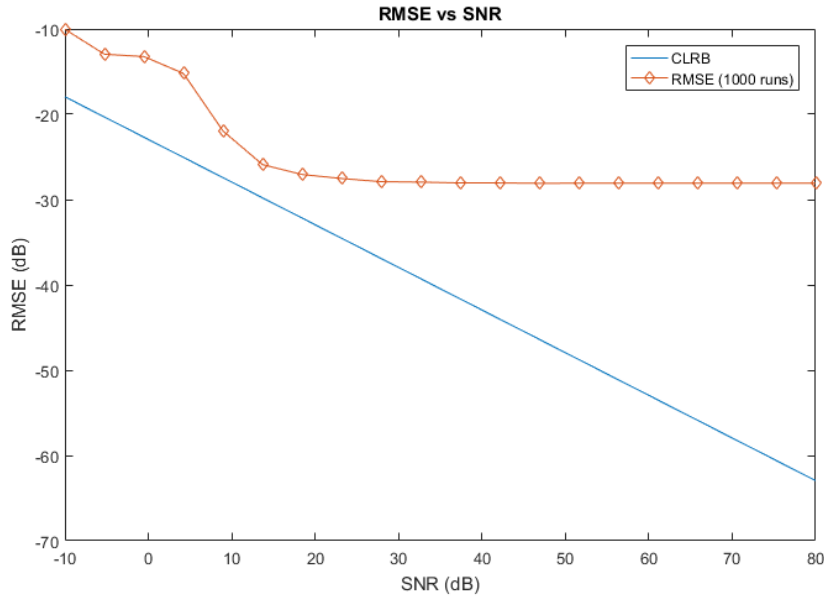
2.3.2 Performance

Figure 2.2: A&M performance vs CRLB

As seen in Figure 2.2 above, the RMSE of the A&M algorithm on its own provides an initial value that is relatively close to the CRLB. However, as the SNR increases, the CRLB decreases linearly but the RMSE only decreases slightly and then hits a plateau and flattens out. Increasing the SNR past 30dB shows no observable increase in performance or accuracy. This lower boundary signifies the algorithm's inability to resolve the frequency spectrum of the real signal any further. This shortcoming and lack of better results is presumed to be at the mercy of spectral leakage effects. This phenomenon will be discussed in detail in the next chapter.

2.4 Cramér–Rao Lower Bound

The Cramér–Rao Lower Bound (CRLB) is widely used as a benchmark to assess the performance of a frequency estimation algorithm. It presents the theoretical lower bound for variance in estimates for any frequency estimator[20]. The CRLB is calculated from the diagonal elements of the inverse of the Fisher information matrix. The CRLB for frequency of a single mode real scalar process in the form $y_t = \cos(\omega_i t + \theta_i) + \epsilon_t$ is proposed by Yao[21] and Rife[22].

$$\lim_{\zeta \to 0} \text{CRLB}(\omega) \approx \frac{12}{SNR_R N(N^2 - 1)} \tag{2.2}$$

where $\zeta \to 0$ eliminates the damping to provide a pure real sinusoid.

Chapter 3

Research Objectives

3.1 Aims

1. To implement accurate frequency estimation

   This will be done through creating and analysing a mathematical signals model. An algorithm will be chosen and refined accordingly

2. To simulate the proposed calibration method

   Using a simulation environment such as Matlab to run the algorithms and simulate test data for inspection and analysis

3. To create a script that is compatible with live data collected from the Bruker Topspin software

   With the goal of complete automation in mind, create an algorithm that is optimised for overall performance using fixed parameters and a posteriori knowledge

Chapter 4

Calibration Method

4.1 Criteria

When considering a calibration method, comparisons can be categorised into three main factors.

1. Efficiency - is the measure of time and how long the calibration process takes. It also considers the the practical and computational complexity of the process to give an indication of how adept it performs and how suitable it is to run on various systems.

2. Accuracy - is the measure of the systematic error of the process. This is defined as the error in the measured results relative to the true value. One of the objectives of the thesis study is to optimise the accuracy to efficiency relationship.

3. Precision - is also a major factor as it governs the random error. This is the error relative to the measured values of repeated experiments. It goes without saying that the calibration process must be repeatable and reliable with minimum errors, both systematic and random.

4.2 Proposed Calibration Method

The proposed calibration method will seek to improve and refine upon the current POPT method in use by implementing proper digital signals processing techniques[23]. As the POPT method is the most recognised and understood method in the NMR field to date, this new proposed method should not only improve the process itself, but also keep to the current standard and require minimal training for existing users. As a benefit, and to address the PulseCal method, this calibration process can be made to be fully automated and invisible to the user if necessary.

In the proposed solution we are aiming to remove the obsolete method of analysing the spectrum by eye and its resulting human and mathematical errors. Instead, it will be replaced with a robust signals processing algorithm for frequency estimation of a sinusoid. Therefore, we will be calculating the pw90 from what can be thought of as the average of periods over time, as opposed to a single period, which would reduce frequency fluctuations, noise and outlier impacts.

Currently the POPT method revolves around correctly estimating the null points of the sinusoid. This estimation can only be improved by increasing the resolution of array spectrum which can only be done by taking more samples. This will linearly increase the time necessary for calibration for accurate results. By using a frequency estimator such as the A&M algorithm, we aim to not only increase the accuracy, but to significantly increase efficiency by reducing the number of samples and one-pulse experiments required. Once an accurate determination of the frequency can be found, converting that into the pw90 value is trivial.

4.3   Spectral Leakage

4.3.1   Theory

A significant, and enlightening, factor that was not recognised or addressed in the proposal is the phenomenon of spectral leakage[24] in the frequency domain. This oversight was the consequence of assuming that a real sinusoid is strictly the addition of a pair of complex conjugate exponential signals, shown in Equation (4.1), which is only true for a continuous time domain. This spectral leakage effect causes spectral peaks to create interference with one another, resulting in significant inaccuracies in standard frequency estimation methods.

$$
\begin{aligned}
x(t) &= Ae^{j2\pi ft} + Ae^{-j2\pi ft} \\
&= s(t) + s^*(t)
\end{aligned}
\tag{4.1}
$$

Spectral leakage occurs due to the finite nature of a simulated or measured signal and the operation of the Fast Fourier Transform (FFT) that implicitly assumes a periodic repetition beyond the measured interval of the signal. Hence, the FFT assumes the signal to be continuous and periodic. Therefore, if the measurement time (the sampling frequency multiplied by the number of samples) is not an integer multiple of the signal frequency, discontinuities will arise at the edges of each period. In the frequency domain of the signal, these discontinuities will result in spectral leakage.

Spectral leakage also occurs in the frequent case of the true signal frequency f_x not being a perfect multiple of the Fourier transform resolution $\Delta f = \frac{f_s}{N}$. This causes the frequency spectrum to have inadequate

resolution to display the frequency in a single bin, which results in the energy of the signal to be leaked into the adjacent bins, causing significant spectral leakage.

In general, an FFT constitutes a default rectangular window on a data stream unless another window has previously been applied. A windowing operation in the time domain translates into a convolution in the frequency domain with the transform of the window function. For the default rectangular window, the transform is in the form of a sinc (sin(x)/x) function, which theoretically has infinite width. Thus, the ripples of these sinc functions will interfere and display as leakage in any spectral peak that isn't perfectly periodic in the FFT's length.

In the case of a real sinusoid as we are interested in, the FFT of the windowed signal will result in a pair of deltas convolved with the sinc from the rectangular window.

4.3.2   Simulation

To observe this effect in action, a simulation[25] can be run with leakage inducing parameters. In this test, a pure sinusoidal signal in generated with a frequency $f_x = 10Hz$ and unit amplitude. The sampling frequency is set to $F_s = 100Hz$, a perfect multiple of f_x, however the experimental run time is set to 0.85 seconds. This will create a finite signal with a non-integer number of wavelengths. The time domain signal is shown below in Figure 4.1.
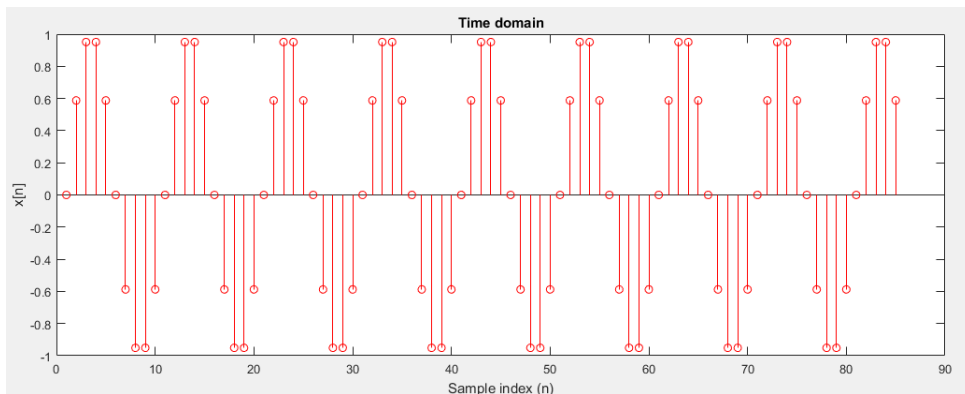

Figure 4.1: Time domain signal

In the first case, shown in Figure 4.2, there is a resolution mismatch between the true frequency of the signal and the frequency resolution of the spectrum when $N = 128$, as $\Delta f = 0.7813Hz$ is not a factor of $10Hz$. As clearly shown, the spectrum cannot accommodate the exact value of $10Hz$. Instead, major spectral leakage is spread across the other bins.
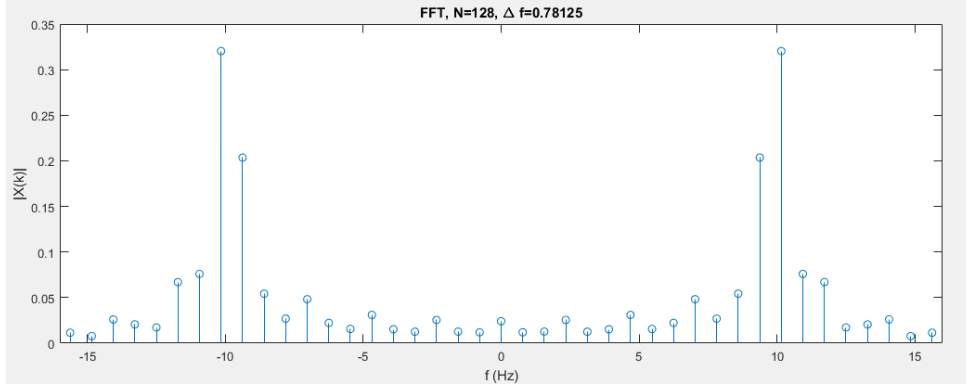
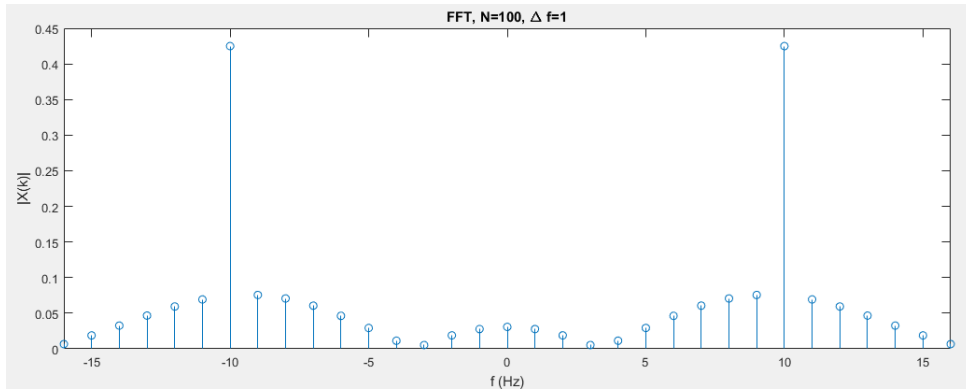Figure 4.2: Resolution mismatch in spectral leakage

Figure 4.3: Windowing effect in spectral leakage

The second case, shown in Figure 4.3 considers the resolution and addresses this by setting $N = 100$, $\Delta f = 1Hz$. However, careful observation will reveal that even with a perfect resolution, there is still a low amount of spectral leakage due to the non-integer wavelength signal and windowing effects.

4.4 Extended Algorithm

Due to the unforeseen effects of spectral leakage, it is apparent that the preliminary assumption, in Equation (4.1), that an estimator for complex exponential signals will work on real sinusoids will no longer be sufficient. The new algorithm for the estimation of the parameters of a real sinusoid in noise[12] developed by Aboutanios, Kocherry and Ye addresses these issues with a refined and extended algorithm to operate ideally on real sinusoidal signals in noise.

$$
\begin{aligned}
x(n) &= a\frac{e^{j\phi}}{2}e^{j2\pi fn} + a\frac{e^{-j\phi}}{2}e^{-j2\pi fn} + w(n) \\
&= Ae^{j2\pi fn} + A^*e^{-j2\pi fn} + w(n) \\
&= s(n) + s^*(n) + w(n)
\end{aligned}
\tag{4.2}
$$

The A&M algorithm is already proven to work perfectly for a complex exponential signal $s(n)$. However, if it is used directly on sinusoidal signal $x(n)$, the leakage effects caused by $s^*(n)$ will result in biased results from the algorithm. The refined estimator, therefore, must estimate the effects of $s^*(n)$ and subtract it from the signal $x(n)$ in each iteration of the dichotomous search process. The entire estimation algorithm can be simplified into the flow chart below in Figure 4.4.
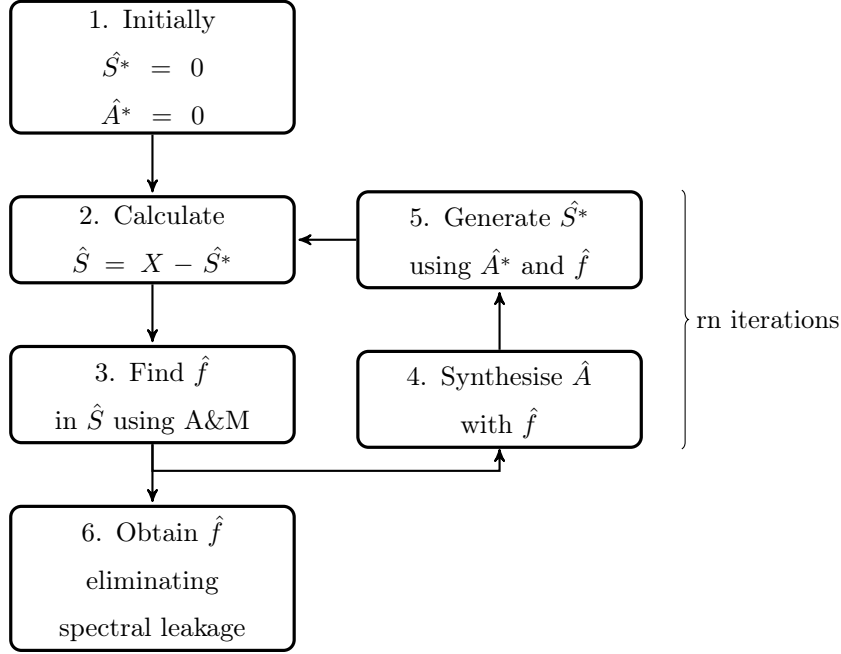

Figure 4.4: Flow chart of extended algorithm

From the flow chart, rn dictates the number of internal iterations of the algorithm. Each iteration includes the calculation of the peak amplitude A^* in the frequency domain and the generation of S^*. At the end of every iteration, $\hat{S}$ is updated by subtracting the estimate of $\hat{S^*}$ from the real signal. After several iterations, interfering spectral leakage effects can be significantly reduced or eliminated.

The procedure for generating S^* begins with the first estimate of the frequency f. The amplitude of the peak in the frequency domain can be expressed as

$$\hat{A} = \frac{1}{N}\left(\sum_{n=0}^{N-1} x(n)e^{-j\frac{2\pi}{N}(\hat{m}+\hat{\delta})n} - \hat{A^*}\frac{1-e^{-j4\pi\hat{\delta}}}{1-e^{j\frac{4\pi}{N}(\hat{m}+\hat{\delta})}}\right)$$

$$\text{new } \hat{A^*} = conj(\hat{A})$$

(4.3)

The new estimate of S^* can then be calculated as

$$\hat{S}^* = \hat{A}^* \frac{1 + e^{-j4\pi\hat{\delta}}}{1 - e^{-j\frac{4\pi}{N}(\hat{m}+\hat{\delta})}} \tag{4.4}$$

Where m is the maximum bin and δ is the frequency residual.

After completely subtracting the S^* component from X, a purely exponential signal is retrieved and can be successfully estimated with the A&M algorithm. The full pseudocode can be viewed below in Table 4.1.

Given	A real sinusoid $x(n), n = 0 \ldots, N - 1$;
Find	$X(k) = \text{FFT}(x)$ and $Y(k) = \|X(k)\|^2$;
Find	$\hat{m} = \arg\max_k Y(k)$, if $\hat{m} \geq \frac{N}{2}, \hat{m} = N - \hat{m}$;
Set	$\hat{\delta} = 0$ and $\hat{A} = 0$;
Loop	For i from 1 to Q, do
	(1) $\tilde{X}_{\pm} = \sum\limits_{n=0}^{N-1} x(n)e^{-j\frac{2\pi}{N}(\hat{m}+\hat{\delta}\pm 0.5)n}$;
	(2) $\hat{\tilde{S}}_{\pm} = \hat{A}^* \dfrac{1 + e^{-j4\pi\hat{\delta}}}{1 - e^{-j\frac{2\pi}{N}(2\hat{m}+2\hat{\delta}\pm 0.5)}}$, and $\hat{S} = \tilde{X}_{\pm} - \hat{\tilde{S}}$;
	(3) $\hat{\delta} = \hat{\delta} + \dfrac{1}{2}\Re\left\{\dfrac{\hat{S}_+ + \hat{S}_-}{\hat{S}_+ - \hat{S}_-}\right\}$;
	(4) $\hat{A} = \dfrac{1}{N}\left(\sum\limits_{n=0}^{N-1} x(n)e^{-j\frac{2\pi}{N}(\hat{m}+\hat{\delta})n} - \hat{A}^* \dfrac{1 - e^{-j4\pi\hat{\delta}}}{1 - e^{-j\frac{4\pi}{N}(\hat{m}+\hat{\delta})}}\right)$;
Find	$\hat{f} = \dfrac{\hat{m} + \hat{\delta}}{N}, \hat{a} = 2\|\hat{A}\|$ and $\hat{\phi} = \angle\hat{A}$.

Table 4.1: Extended algorithm pseudocode

4.5   Block Diagram

To easily and visually compare the principles of operation between pulse calibration methods, block diagrams have been presented in Figures 4.5, 4.6 and 4.7. From these, it is clear to see where the complexities in each method reside. In both the POPT and PulseCal methods, the complexity is within the practical aspect in the form of requiring large repetitions of experiments with POPT or relying heavily on complex experimental setup and analogue electronics. However, the proposed method raises its complexity in the post-collection signals processing stage, which produces a much simpler overall system and reduces the efficiency impact.
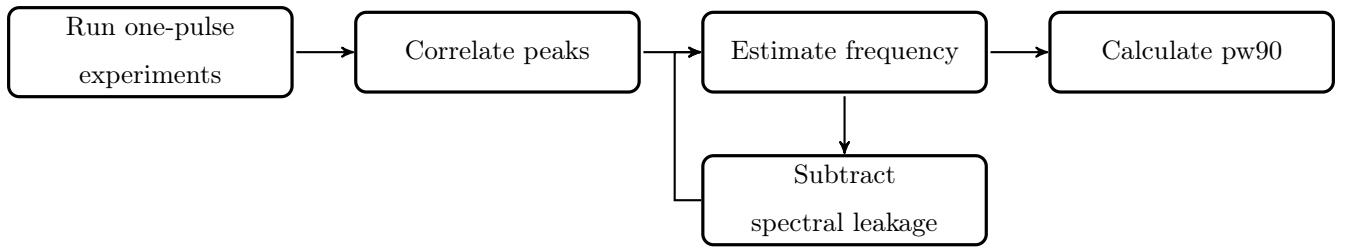
Figure 4.5: Block diagram of proposed method

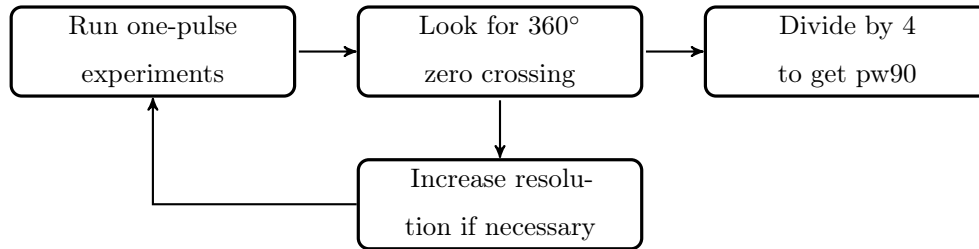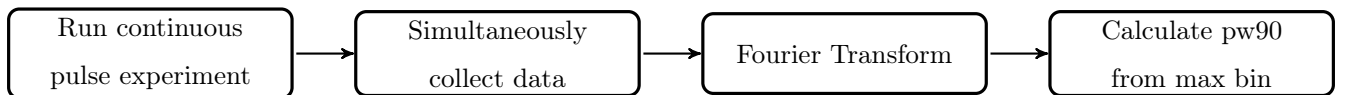Figure 4.6: Block diagram of POPT method

Figure 4.7: Block diagram of PulseCal method

4.6   Potential Advantages Summary

- Greater accuracy

- Reduced total calibration time

- Independent of linear amplifier induced errors

- Optimised efficiency to accuracy trade-off

- Simplified experimental procedure as complexity is in post collection processing stage

- Completely automated process

Chapter 5

Signals Modelling

5.1 Mathematical Modelling

For simplicity without loss of generality, assume all calculations are based on a single line FID unless stated otherwise.

5.1.1 Free Induction Decay

The FID received in the xy-plane due to the precession of the magnetisation vectors follows the co-ordinates of a circle, such that:

$$s_x = A\cos(2\pi f t) \text{ and } s_y = A\sin(2\pi f t) \tag{5.1}$$

where A is the overall amplitude of the signal.

Combining the two we get:

$$\begin{aligned} s(t) &= s_x + js_y \\ &= A(\cos(2\pi f t) + j\sin(2\pi f t)) \\ &= Ae^{j2\pi f t} \end{aligned} \tag{5.2}$$

Also, there is an exponential decay rate factor that depends on the T_2 relaxation time

$$e^{-\eta t}, \text{ where } \eta = \frac{1}{T_2} \tag{5.3}$$

The FID signal can thus be written as:

$$s(t) = Ae^{j2\pi ft}e^{-\eta t} + w(t) \text{ , for a single spectral line}$$

or

$$= \sum_i A_i e^{(-\eta_i + j2\pi f_i)t} + w_i(t) \text{ , for multiple spectral lines}$$

(5.4)

where $w(t)$ is additive white Gaussian noise.

5.1.2 The Fourier Transform

To transform from the FID (time domain) into the desired spectrum (frequency domain) we use a process known as the Fourier transform.

$$
\begin{aligned}
S(\omega) &= \int_0^\infty s(t)e^{-j\omega t}dt \\
&= \int_0^\infty Ae^{j2\pi ft}e^{-\eta t}e^{-j\omega t}dt \\
&= \int_0^\infty Ae^{[-j(\omega - 2\pi f) - \eta]t}dt \\
&= A\left[\frac{e^{[-j(\omega - 2\pi f) - \eta]t}}{-j(\omega - 2\pi f) - \eta}\right]_0^\infty \\
&= \frac{A}{j(\omega - 2\pi f) + \eta} \\
\\
&= \frac{A[-j(\omega - 2\pi f) + \eta]}{(\omega - 2\pi f)^2 + \eta^2}
\end{aligned}
$$

(5.5)

This gives us the frequency spectrum in the form

$$S(\omega) = \frac{A\eta}{(\omega - 2\pi f)^2 + \eta^2} + j\frac{-A(\omega - 2\pi f)}{(\omega - 2\pi f)^2 + \eta^2}$$

(5.6)

Where the real part is known as the absorption and the imaginary part is known as the dispersion. Both absorption and dispersion have a Lorentzian lineshape with a full-width at half-maximum of 2η rad s^{-1} or $\frac{\eta}{\pi}$ Hz.

5.1.3 Discrete Signals

When working with digital equipment, signals are not continuous, instead they are a series discrete values sampled at a certain frequency f_s. This means that both the FID and the spectrum must be represented as their discrete counterparts. Assuming that the sampling frequency is sufficient to avoid aliasing, the spectrum sampled in the frequency domain is synonymous to a signal sampled in the time domain and set through the discrete Fourier transform (DFT).

For the FID, the signal is sampled at every interval $t = nT$, where T is the sampling period equal to $\frac{1}{f_s}$ and n is the index of the sample in the time domain.

$$s(t) \Rightarrow s[n] = Ae^{j2\pi fnT}e^{-\eta nT} \tag{5.7}$$

Similarly, the frequency spectrum is also sampled with intervals $\omega = \frac{2\pi k}{N}$, where N is the total number of samples used in the DFT, which is also the total number of samples in the collected FID, and k is the index of the sample in the frequency domain. Assuming bandlimited and satisfying the Nyquist sampling criterion, therefore no aliasing.

$$S(\omega) \Rightarrow S[k] = \frac{A\eta}{[2\pi(\frac{k}{N} - f)]^2 + \eta^2} + j\frac{-A[2\pi(\frac{k}{N} - f)]}{[2\pi(\frac{k}{N} - f)]^2 + \eta^2} \tag{5.8}$$

5.1.4 Creating the Full Spectrum

We will mainly be focusing on the real part of the spectrum as that gives us the most valuable and cohesive information.

$$S_r[k] = \frac{A\eta}{[2\pi(\frac{k}{N} - f)]^2 + \eta^2} \tag{5.9}$$

To change from the spectrum consisting of a single spectral line to multiple lines is simply a matter of summing the spectra of all the included lines.

$$S[k] = \sum_i \frac{A_i\eta_i}{[2\pi(\frac{k}{N} - f_i)]^2 + \eta_i^2} \tag{5.10}$$

The main variable of this study is the pulse width τ, which directly influences the amplitude of the signal.

$$A \Rightarrow A(\tau) \tag{5.11}$$

Then the array spectrum can be thought of as a function of both variables

$$R[k, \tau] = \sum_i \frac{A(\tau)\eta_i}{[2\pi(\frac{k}{N} - f_i)]^2 + \eta_i^2} \tag{5.12}$$

Thus the function with appended spectra dependent on the pulse width is

$$R_k[\tau] = \sum_i \frac{A(\tau)\eta_i}{[2\pi(\frac{\tau-k}{N} - f_i)]^2 + \eta_i^2} \text{ , for k} = 0, 1, 2 \ldots \text{N-1} \tag{5.13}$$

As seen previously in the POPT method, the amplitude of the FID naturally tends to a sin wave. As such, the estimated signal x, based around discrete points of A, will also tend to a sinusoid. Consequently, it will be a function of τ of the form:

$$x(\tau) = A_{max} \sin(2\pi f_c \tau) \tag{5.14}$$

where A_{max} is the amplitude of $A(\tau)$ multiplied by some scaling factor dependent on the decay rate and, therefore:

$$\text{pw90} = \tau_{90} = \frac{1}{4f_c} \tag{5.15}$$

5.2 Matlab Models

In parallel to modelling the signals, a simplified baseline for a Matlab script to simulate test data has been conducted to visually display the models. It performs a simplified POPT experiment whilst excluding noise and environmental effects to provide a clear image. The full code can be found in Appendix 2. For an example, an FID response has been generated, in Figure 5.2 consisting of two measured nuclei responses with arbitrarily assigned properties shown in Figure 5.1.
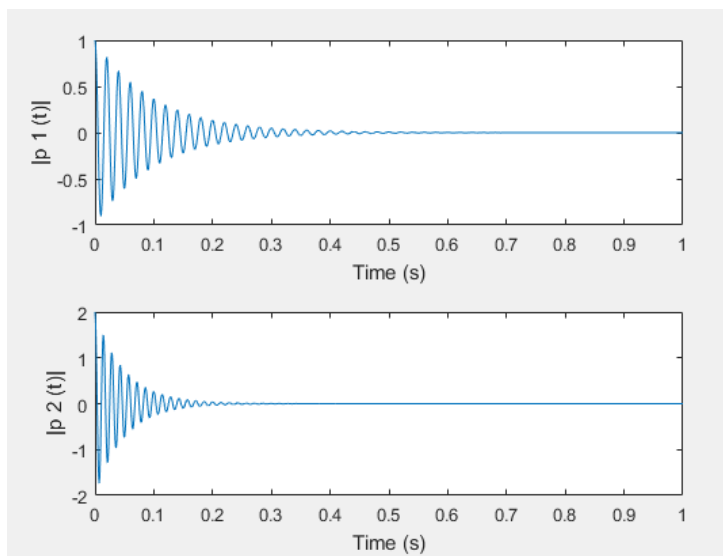

Figure 5.1: Simulated FID components
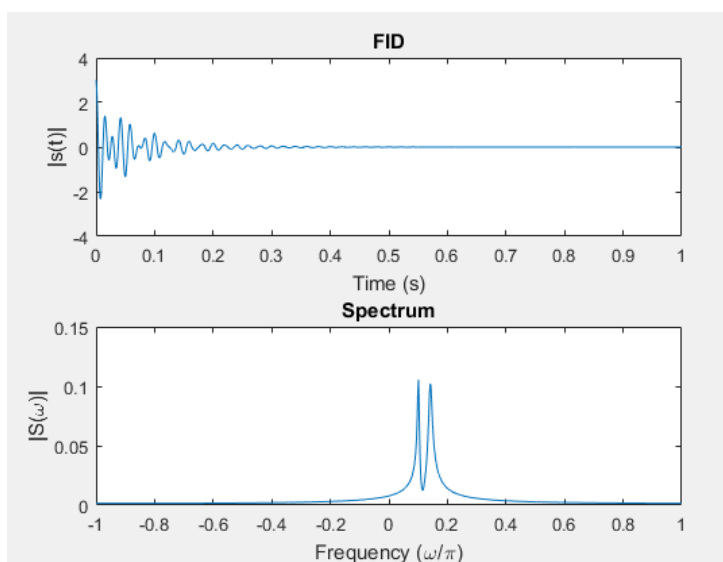
Figure 5.2: Simulated FID and resulting spectrum

The FID signal is passed through the fast Fourier transform (FFT), a computationally more efficient DFT, and the resulting frequency spectrum is also shown in Figure 5.2 above.

To simulate the POPT experiment, the amplitude of the FID components are varied accordingly against changes in the theoretical pulse width and the spectrum is taken and compared for each value. To make process and pulse width correlation apparent and easy to understand, both a 2D and a 3D map of the array of spectra is presented.

Figure 5.3: 2D pw array spectrum

Figure 5.4: 3D pw array map

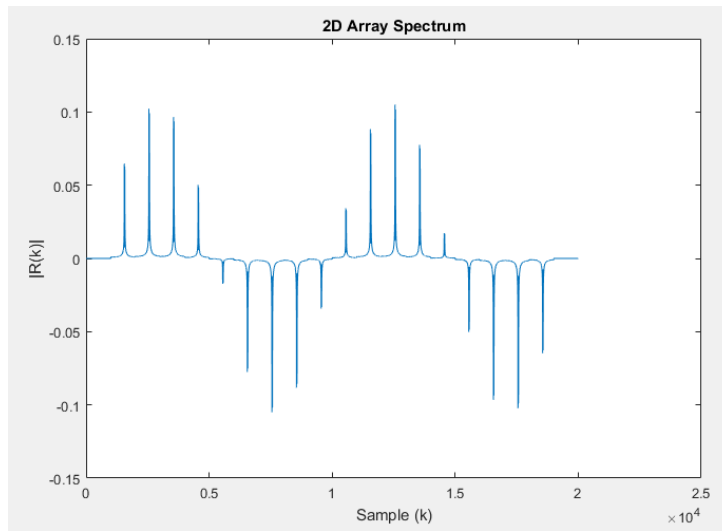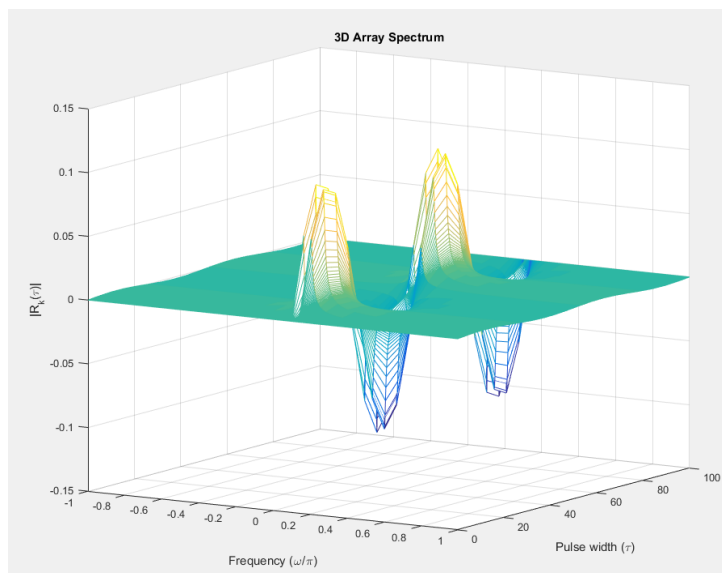The 2D array spectrum in Figure 5.3 roughly shows a sinusoidal envelope between the peaks of each Lorentzian lineshape as expected. The 3D array map in Figure 5.4 is much more insightful and intuitive. Looking from the magnitude against frequency plane, the image would simply by that of the spectrum shown in Figure 5.2 previously. However, including the third dimension of pulse width causes the amplitudes of the spectra to vary in the magnitude against pulse width plane, and when viewed from that plane, the image is clearly a sinusoid. To show, the two sinusoids caused from the two correlating peaks in the spectra, can be extracted and displayed in a 2D format seen below in Figure 5.5.
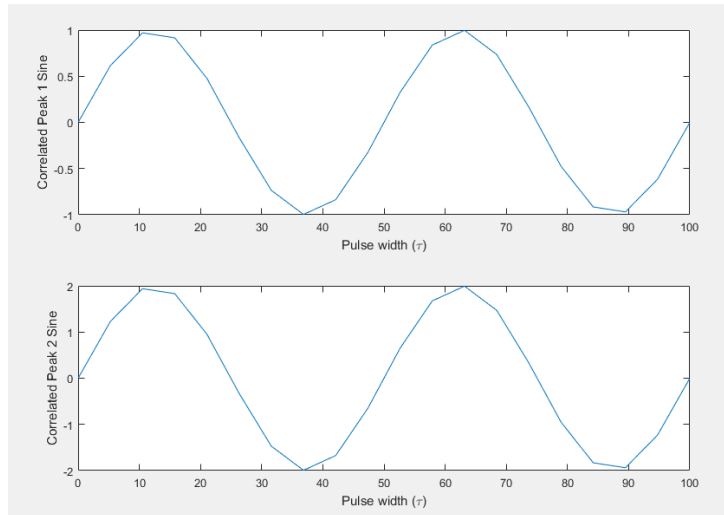

Figure 5.5: Extracted sinusoids of interest

It is precisely this real sinusoid that is the subject of the frequency estimation algorithm. The true signal will obviously become imprecise as the number of samples in reduced and far less ideal once noise, environmental effects, spin phenomena and other destructive effects are introduced.

Chapter 6

Simulated Results

Performance of this new proposed estimator can be tested through a Monte Carlo algorithm and comparison to the CRLB. The simulated results are shown using the estimator on real sinusoidal signals with certain varying characteristics. The results are calculated and displayed in a Root Mean Squared Error (RMSE) format in the units of decibels. Every Monte Carlo simulation is averaged from 1000 runs to improve accuracy and reliability.

6.1   Performance with varying SNR

The first simulation is run with varying the SNR while checking the RMSE of the results. For each SNR value, a series of frequencies around the expected real world sample of a pw90 in the range of 5us to 20us are simulated and the RMSE is taken as the mean of the collection of results from all those frequencies.

6.1.1   Calculation of CRLB

Starting with a discrete sinusoidal signal with added white Gaussian noise.

$$s[n] = A\sin(2\pi fnT) + w[n] \text{ , for n = 0, 1, 2 } \ldots \text{N-1} \tag{6.1}$$

The parameter vector

$$\theta = \begin{bmatrix} A \\ f \end{bmatrix} \tag{6.2}$$

Therefore, the Fisher Information Matrix (FIM) is calculated to be

$$[I(\theta)]_{i,j} = \frac{1}{\sigma^2} \left(\frac{\delta s_\theta}{\delta \theta_i} \right) \left(\frac{\delta s_\theta}{\delta \theta_j} \right)^T$$

$$= \frac{1}{\sigma^2} \sum_{n=0}^{N-1} \left(\frac{\delta s_\theta}{\delta \theta_i} \frac{\delta s_\theta}{\delta \theta_j} \right) \tag{6.3}$$

$$= \begin{bmatrix} \frac{N}{2\sigma^2} & 0 \\ 0 & (2\pi)^2 \frac{A^2}{2\sigma^2} \left(\frac{N(N^2-1)}{12} \right) \end{bmatrix}$$

The CRLB's of the corresponding parameter estimators are then taken from the diagonal elements of the inverse of the FIM

$$V = [FIM]^{-1} = \begin{bmatrix} \frac{2\sigma^2}{N} & 0 \\ 0 & \frac{2\sigma^2}{(2\pi)^2 A^2} \left(\frac{12}{N(N^2-1)} \right) \end{bmatrix} \tag{6.4}$$

For the CRLB of frequency estimation, we take the second diagonal (lower right) element of the matrix. Hence,

$$CRLB(f) = \frac{2\sigma^2}{(2\pi)^2 A^2} \left(\frac{12}{N(N^2-1)} \right)$$

$$= \frac{12}{(2\pi)^2 \; \text{SNR}_R \; N(N^2-1)} \; , \; \text{where SNR}_R = \frac{A^2}{2\sigma^2} \tag{6.5}$$

6.1.2 Simulation Results

Figure 6.1 shows the performance of the frequency estimator against the CRLB. In this trial, the number of internal iterations is set to $rn = 25$ and the data is synthesised with only 4 data points. From the graph, it can be clearly seen that when the SNR is large enough, the RMSE will follow close to the CRLB. At the tail of the RMSE, the graph is seen to begin to flatten out and diverge away from the CRLB, meaning that the variance is unable to decrease steadily despite the increased SNR. This is most likely due to the performance being limited by the number of internal iterations rn.

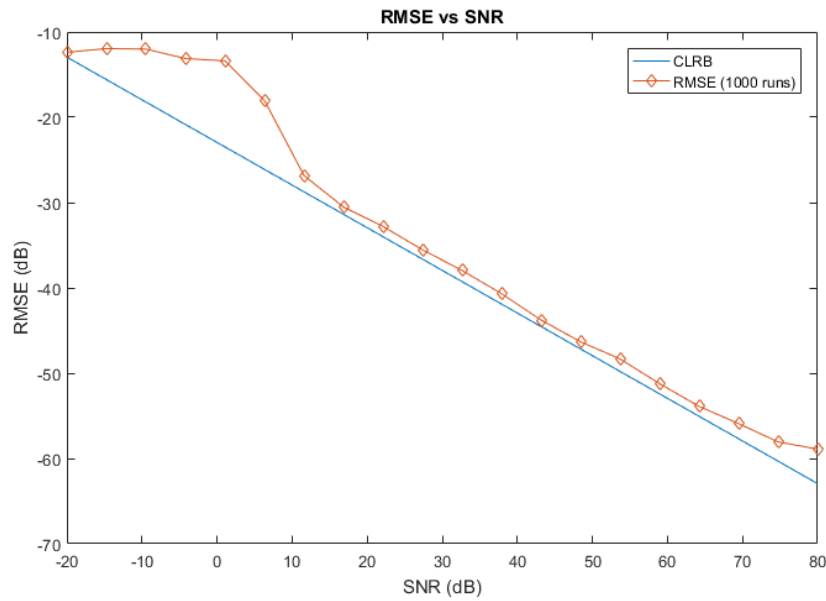

Figure 6.1: Estimator RMSE and CRLB, 4 data points, rn = 25

These issues can easily be addressed by increasing the number of data points, iterations, and overall runs, as seen in the following section. However, these will come at the cost of increased process time and reduced efficiency. For the purpose of NMR pulse calibration, standard NMR machines run within the SNR range of 30dB to 80dB.

6.2 Optimising Parameters

6.2.1 Internal Iterations

As mentioned previously, the plateauing and divergence from the CRLB is exaggerated in Figure 6.2 as the number of internal iterations rn varies. It can be seen here that as the number of iterations increases, the RMSE will follow the CRLB for a larger range of SNR. Specifically, it increases the upper bound SNR value before divergence. For the expected upper SNR value of 80dB, $rn = 25$ iterations is considered to be sufficiently close to the CRLB without any unnecessary reduction in efficiency.
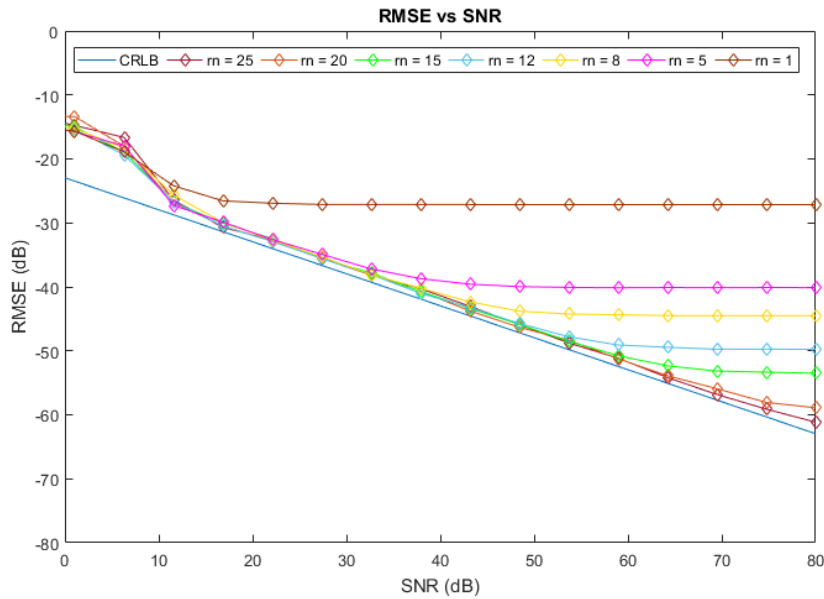
Figure 6.2: Effect of changing internal iterations rn

6.2.2 Number of Experiments

One of the main advantages of the newly proposed calibration method is the ability to optimise the efficiency to accuracy trade-off. The most efficiency impacting factor in the calibration process is with the number of one-pulse experiments conducted to generate the data points necessary for the frequency estimation. Each data point is equivalent to a single one-pulse experiment, thus the number of data points collected is linearly scaled with the process time to run a one-pulse experiment. According to the CLRB formula in Equation (6.5), and the effectiveness of the algorithm, an increase in data points correlates with an increase in accuracy. In this nature, there is an accuracy (effectiveness of algorithm) to efficiency (number of one-pulse experiments) relationship.
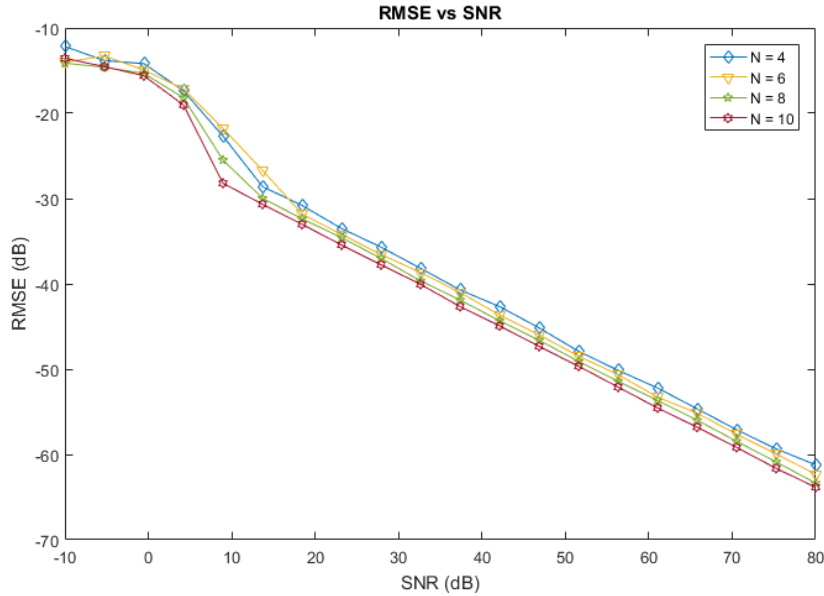
Figure 6.3: Effect of changing number of experiments N

Figure 6.3 contrasts the accuracy, in RMSE, of the new frequency estimator with various signals of N = 4, 6, 8, and 10 data points. It can be clearly seen that increasing the number of data points results in a decrease in RMSE, which stabilises after 20dB SNR, and, therefore, an increase in overall accuracy. This aligns with the expectations, and a cost function can be calculated.

To quantify the accuracy-efficiency relationship and formulate a cost function, the SNR is fixed to a stable value of 50dB and internal iterations rn = 25, and the Monte Carlo algorithm is run with RMSE against the number of one-pulse experiments (N). With these conditions, the graph in Figure 6.4 is produced. Only the range of 4 to 13 experiments is considered because the estimator is significantly unstable and unreliable with less than 4 points and going above 13 would cause the process to become too inefficient for the goals at hand. For future work, if there is a requirement for a calibration process to provide maximum possible accuracy without regards to efficiency or automation, larger numbers of experiments can be explored.
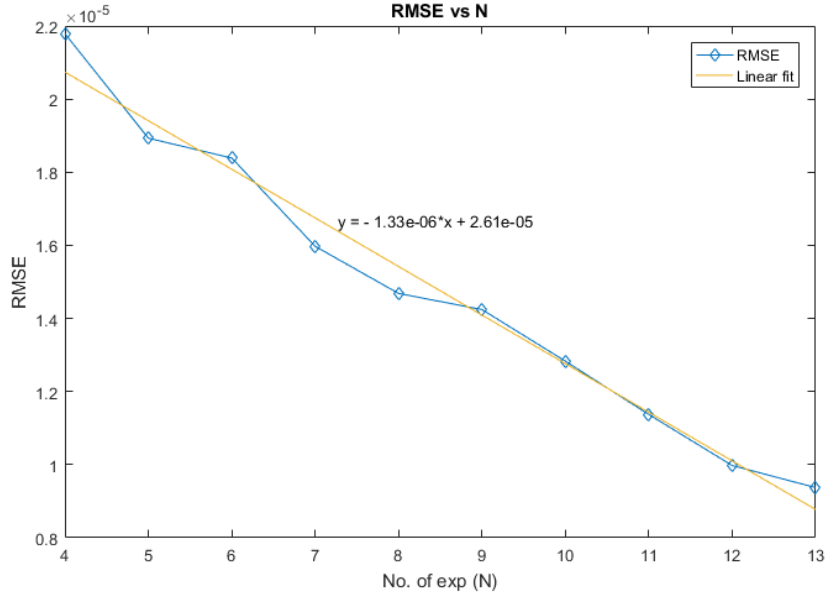
Figure 6.4: Accuracy vs Efficiency

Surprisingly, Figure 6.4 shows a decently linear relationship between RMSE and N, as opposed to the cubic suggested by the CRLB. The straight line shows the linear curve of best fit and is used as an approximation of the cost function.

Therefore, the cost function is expressed as

$$RMSE = -1.33 \times 10^{-6} \times NoOfExperiments + 2.61 \times 10^{-5} \qquad (6.6)$$

As a decreasing linear function, accuracy is maximised when RMSE is minimised, and number of experiments is maximised. However, when the rate of decrease of RMSE with respect to N is considered, the gradient of -1.33×10^{-6} is relatively much smaller than the initial value of 2.61×10^{-5} or the value 2.08×10^{-5} at the lower limit N = 4. At a ratio of almost 1:20, this gradient can almost be considered to be insignificant over a small range. Especially considering the linear increase in time cost as N increases. Since the cost function is so heavily weighted on the efficiency side, with large increases in experiment time providing only small increases in accuracy, the optimal balance occurs at the lowest practical value of $N = 4$.

6.2.3 Pulse Width Increment

When running the Monte Carlo algorithm with RMSE against true pw90 values with varying pulse width increment values, it became apparent that some increments would provide better performance than others. This is theoretically due to the resolution of the frequency spectrum and the distance between the spectral peaks. This distance is formed from a ratio between the signal frequency and the sampling frequency. The effects of spectral leakage from one peak to the other is minimised when the distance between is maximised. This occurs when the sampling frequency is 4 times the sampling frequency as the spectrum is mirrored and periodic.

To investigate the optimal pulse width increment for signals ranging between 5 and $20/mus$, a simulation was run with a fixed number of data points $N = 4$ whilst varying the pulse width increment, $pwinc$, from 5 to $15\mu s$. The results, shown below in Figure 6.5, rectify this puzzle. The differing graphs show a similar behaviour to the internal iterations test, with larger values of $pwinc$ causing the curve to plateau earlier and accuracy to suffer. From the graph, pulse width increments of $5\mu s$ and $7\mu s$ provide the best accuracy by a significant difference from the higher values.
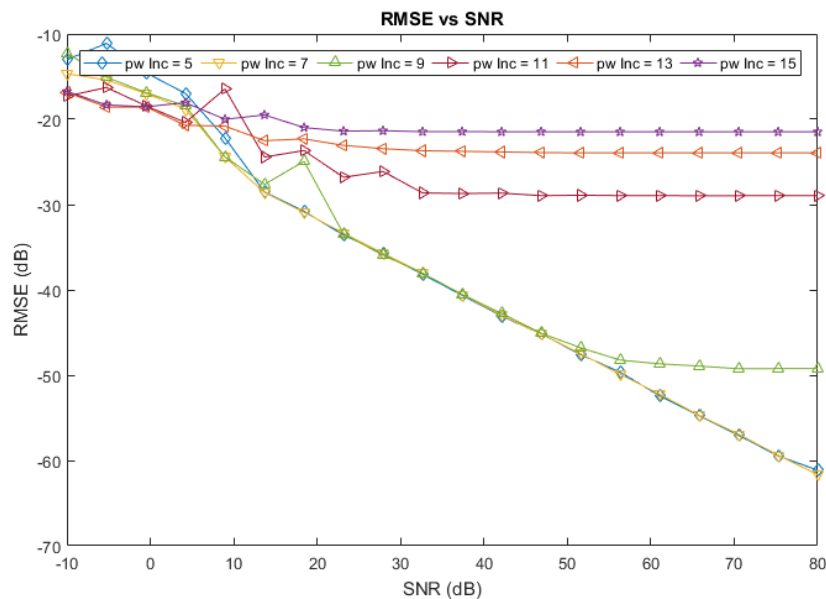
Figure 6.5: Effect of changing pw increment value (pulse width resolution)

Chapter 7

Practical Results

7.1 Initial Testing

As an initial trial, a demonstrative experiment was conducted of both the POPT and PulseCal in practical environments, calibration methods. Both calibrations were performed consecutively under similar conditions using a 600MHz NMR instrument. The sample was a mixture of 2mM Sucrose, 0.5mM DSS and 2mM NaN_3 dissolved in a solution of 90% H_2O and 10% D_2O, a standard sample for water suppression experiments[26].

(a) FID

(b) Pulse width array spectrum
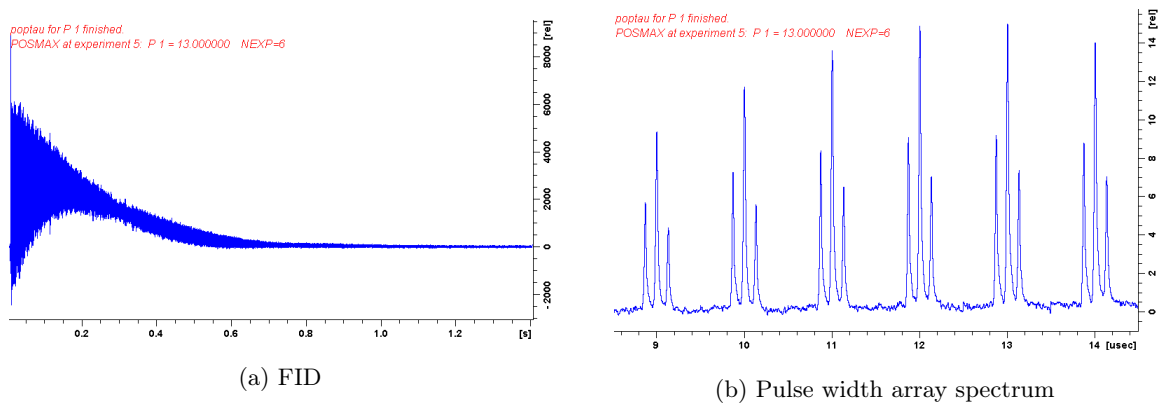
Figure 7.1: POPT experiment results

Figures 7.1a and 7.1b show the resultant FID and spectrum, respectively, of the POPT calibration method. Due to time limitations of the demonstration, we were only able to collect a small set of 6 samples with the pulse width beginning at $9\mu s$ and increasing in increments of $1\mu s$. Even from this dataset, it can be seen that the pw90 would lie near between $12\mu s$ and $13\mu s$. The total time to collect 6 samples was approximately 5 minutes which is ridiculously inefficient, considering a full calibration would take upwards of 20 samples for just a rough estimate.

(a) FID
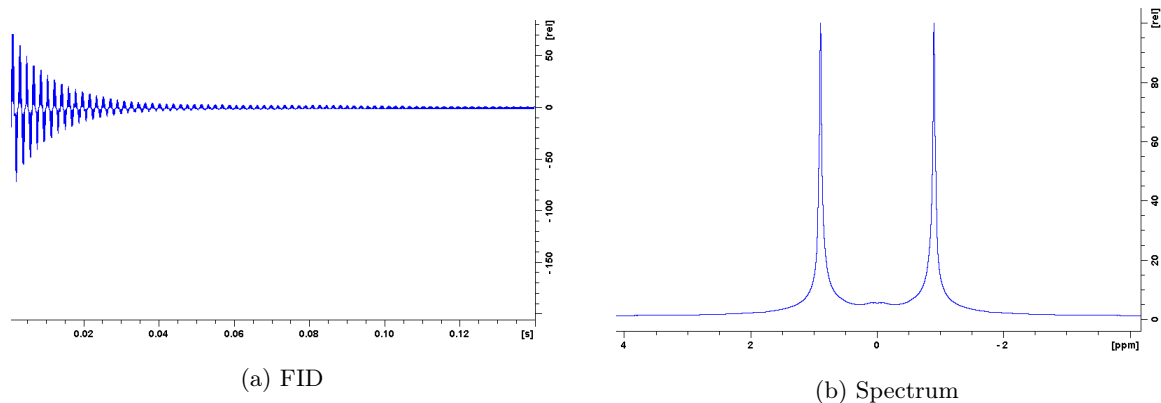
(b) Spectrum

Figure 7.2: PulseCal experiment results

The FID and spectrum of the PulseCal experiment is shown in Figures 7.2a and 7.2b, respectively. This is usually invisible to the user as an automated process and resulted in an estimated pw90 of $11.6\mu s$ which is a fairly large discrepancy against the POPT results. This method only took approximately a minute to complete, however, an error of up to 10% would be dangerous in advanced NMR experiments where errors will compound and accumulate. The proposed calibration method output an estimated pw90 of $12.36\mu s$ which from observing the POPT spectrum, looks to be far more accurate than both the POPT and PulseCal method.

7.2 Spectral Peak Amplitude vs Integral

One major decision that must be made when utilising the data outputted from the Bruker Topspin software with POPT spectra is in the peak correlation. Topspin has native support with an in-built algorithm to select peaks from a spectrum. This data is presented in two ways, either as the amplitude, height of the peaks, or as the integral, area under the peaks. The waveforms generated by either set of data points is shown below in Figure 7.3.

After normalising the values, it is apparent that both curves steadily decay over the number of experiments. This can be easily attributed to T_1 abuse and radiation damping effects that are accumulating as the sample is being re-irradiated continuously as previously shown in Figure 2.1. Despite the decay, it can be seen that the integral correlation loses its pure sinusoidal characteristics at a much more rapid rate than the amplitude correlation. Therefore, the use of amplitude correlation is prioritised for testing.
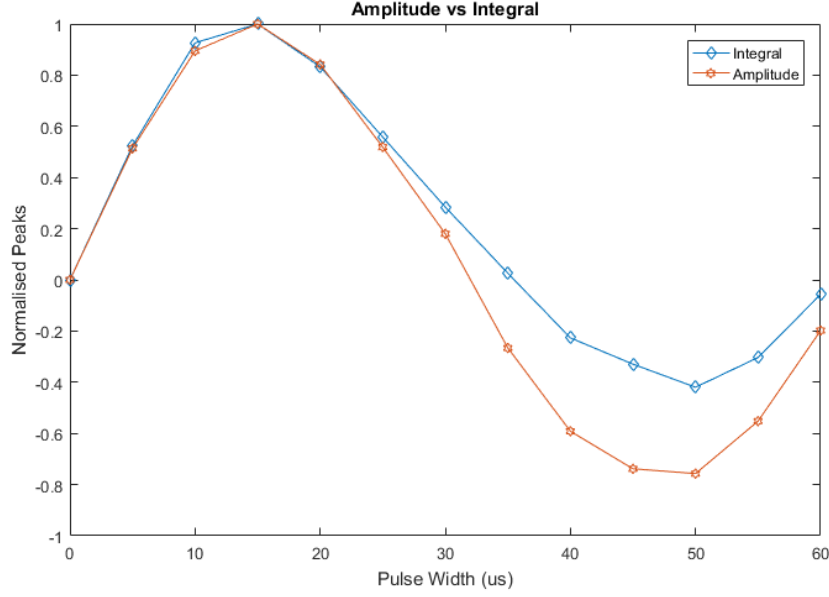
Figure 7.3: Amplitude vs Integral

7.3 Process Time

To consider the total time taken to calibrate, the practical time is taken from the POPT method as they share the same practical method. The post collection processing time is measured with the timer tool in Matlab.

$$TotalCalibrationTime = NoOfExp \times NoOfScans \times \left(\frac{TD}{2SW} + Delay \right) + ProcessingTime \quad (7.1)$$

Where NoOfExp is the number of one-pulse experiments conducted, NoOfScans is the number of scans within each experiment to increase SNR. SW is the sweep width and TD is the size of the fid which both contribute together as the amount of time allocated for data acquisition. Delay is the sufficient length of relaxation time to avoid T_1 abuse. On average, we calculate the practical time to take approximately 30 seconds to 1 minute per experiment and the processing time in Matlab to be 0.015 seconds. The processing time is rendered insignificant in the total calibration time, so Equation (7.1) can be simplified to:

$$TotalCalibrationTime \approx NoOfExp \times NoOfScans \times (AcqTime + Delay) \quad (7.2)$$

35

Chapter 8

Discussion

8.1 Optimised Pulse Calibration Process

After various testing and optimisation of parameters, a final complete pulse calibration method is formulated. Currently, with the a posteriori knowledge considered as the expected pw90 values lie within $5\mu s$ and $20\mu s$ and the standard SNR of NMR machines range from 30dB to 80dB. To be considered as an automated process, the parameters must be fixed and optimised for overall performance across expected ranges. Two sets of optimised values are presented, one for the simulated data and one for real practical data. The differences are due to the unforeseen and unaccounted plethora of effects and non-ideal conditions on real NMR experiments.

Parameter	Optimised Theoretical Value	Optimised Practical Value
Number of Experiments	4	4
PW Increment	$5(\mu s)$	$15(\mu s)$
Min PW	$5(\mu s)$	$15(\mu s)$
Number of Scans	N/A	1
Sweep Width	N/A	0.75ppm
Size of FID	N/A	2048
Acquisition Time	N/A	2.27s
T_1 Delay	N/A	10s
Run Time per One-pulse Experiment	N/A	∼1min
Peak Correlation	Amplitude	Amplitude
Internal Iterations rn	25	25

Table 8.1: Optimised parameters

8.2 Comparison with Existing Methods

8.2.1 Theoretical Comparison

Theoretically, the proposed method should prove to be both more accurate than PulseCal and much more efficient than POPT. All the parameters can be controlled and, therefore, the proposed method can be made to sit on the theoretical optimised trade-off point. In contrast, the POPT method relies heavily on user experience, reaction time and cognitive ability which cannot be controlled and difficult to be measured or reliable. This causes it to be radically inefficient compared to any computer automated process, as expected. As the number of full wavelengths for the POPT method increases, the accuracy increases as the noise is averaged over a larger set. Thus, the variance decreases proportionally to $\frac{1}{N}$, where N is the number of full wavelengths. In comparison, the new proposed method is shown to follow closely to the CRLB with correct conditions, which achieves a variance proportional to $\frac{1}{n^{3/2}}$, where n is the number of one-pulse experiments, showing an improvement in accuracy with increasing samples.

On the other hand, the PulseCal method also contains substantial dependencies. PulseCal is a highly practically complex method and relies on many analogue hardware components to measure and calculate parameters. This is an issue especially for calibration, which is a very sensitive process, due to the non-ideal quality of components and their depreciation over time. The main focus point in this comparison against PulseCal is in its fundamental dependency on linear amplifiers. Due to the nature of PulseCal, the final pw90 value is calculated assuming a linear power relationship. Once the linear amplifier has acquired non-linear properties, this assumption fails to hold and the calibration will be incorrect. This is a problem that POPT and the proposed method do not share as, even if the components are not ideal, the independently calculated pw90 value will still be correct for that sample run on that NMR machine under those conditions.

8.2.2 Results Comparison Table

Inherently, it is extremely difficult to assess the true practical accuracy of a calibration process as there is no baseline or fixed reference point without prior given information. As with most experiments, NMR calibration data is not usually saved and there is currently no publicly available database or set of known pw90 for samples. Therefore, a comparison of calibration results between different methods is presented instead. Although it may not provide significant information to assess individual accuracy, it may be useful to compare and contrast the methods under various conditions to see similarities and judge precision.

From Table 8.2, the proposed calibration process using amplitude correlation consistently produces a pw90 value with a deviation that sits between the POPT and PulseCal values. This proves many of the theories mentioned previously if POPT is considered to be the baseline as it contains observable results and good estimate of an approximate pw90. PulseCal results can be seen to differ quite significantly from the baseline POPT approximations which shows the potential performance impact due to linear amplifier degradation. Dr. Donald Thomas and Dr. James Hook, of the Mark Wainwright NMR facility, have confirmed that the linear amplifier and electronics of the machine used to acquire these results has been in use for over 6 years and is definitely prone to non-linear characteristics.

From the collected results, it seems that in the practical setting, using amplitude correlation of 4 experiments and setting a pw increment of $15\mu s$ starting at a minimum of $15\mu s$ provides the closest results to the observable waveform. This is surprising as it even outperforms the $5\mu s$ increments for 12 experiments which was simulated to have the maximum accuracy. The optimal practical parameters have been logged Table 8.1.The integral correlation results can be treated as outliers and disregarded as their performance is proven to be unacceptable and even incompatible with the frequency estimation algorithm in certain cases such as tests 6 and 7.

Interestingly, the severity of the need for an accurate calibration process presents itself in the data. Tests 2-4 and 5-7 were both conducted on the same sample with the same respective parameters at different occasions. The significant difference in the results highlights the requirement for calibrating per sample per machine per occasion, as a change in any of these can cause a different pw90 value. Tests 8 and 9 were conducted with a low spectrum resolution of 2048 as opposed to the 65,536 of tests 1-7. This resulted in a decrease in run time per one-pulse experiment by half to approximately a minute. The POPT spectra used for these tests is given in Figures 8.1 and 8.2.

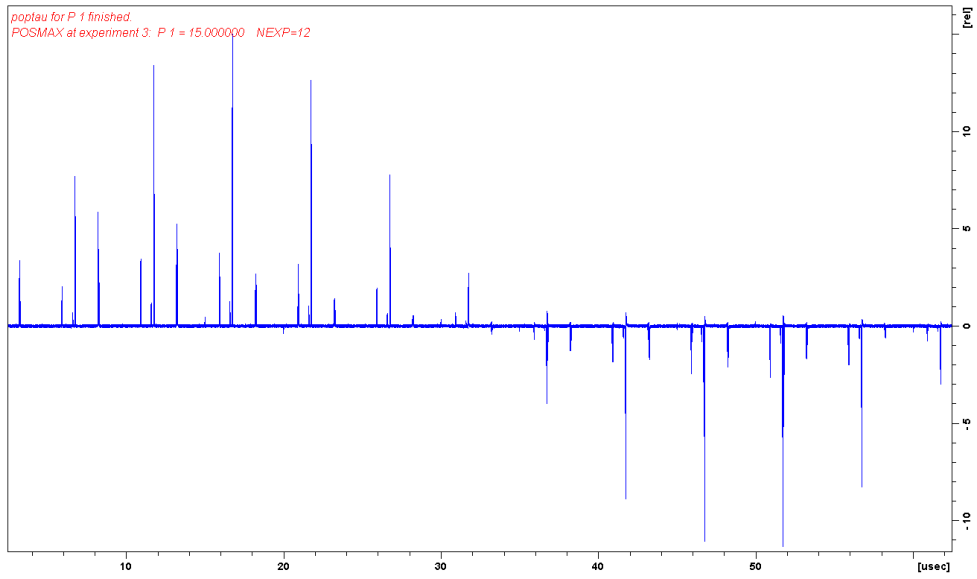| Test	NoOfExp	pw inc (μs)	POPT (μs)	PulseCal (μs)	New (Amp) (μs)	New (Int) (μs)
1	6	1 (min 9)	12.5	11.63	12.36	17.33
2	12	5 (min 5)	15	16.65	15.97	18.82
3	5	15 (min 5)	15	16.65	15.48	22.34
4	4	15 (min 15)	15	16.65	15.35	26.2
5	12	5 (min 5)	14	12.71	13.18	9.27
6	5	15 (min 5)	14	12.71	13.17	N/A
7	4	15 (min 15)	14	12.71	13.73	N/A
8	12 (low res)	5 (min 5)	14	12.71	13.2	13.33
9	4 (low res)	15 (min 15)	14	12.71	14.57	11.62

Table 8.2: Results comparison
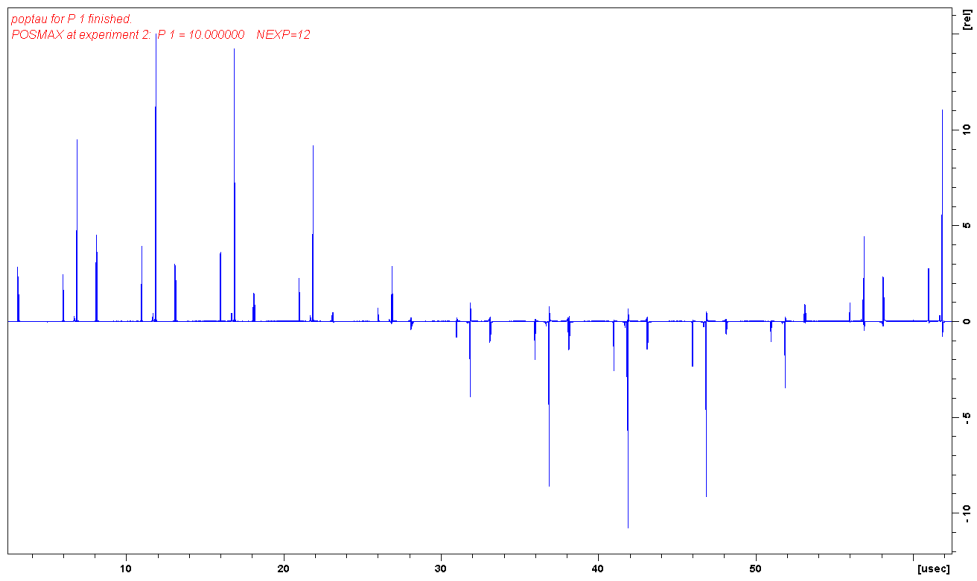
Figure 8.1: POPT spectrum for tests 2-4

Figure 8.2: POPT spectrum for tests 5-9

39

8.2.3 Efficiency Comparison Table

Both POPT and the proposed method utilise the same function of time that is linearly dependent on the number of one-pulse experiments run to collect data. The difference is that the proposed method can operate efficiently and accurately with only 4 one-pulse experiments, whereas the POPT method requires significantly more. Customarily, two sets of experiments must be run for POPT. Once with larger spacing to approximate the region of the 360° zero crossing, followed by a finer set of experiments run between the two pulse width values adjacent to the zero crossing point to create better resolution around the target area. These 2 sets can add up to 20 one-pulse experiments depending on the user's experience and a posteriori knowledge.

On the other hand, PulseCal is based upon completely difference principles and is much more practically complex and hardware dependent. Due to its continuous one-scan nature, it is extremely efficient with most calibration times taking between 45 seconds to a minute in total.

In testing, with the optimised practical parameters from Table 8.1, one-pulse experiments took roughly a minute. Therefore, Equation (7.2) of the total calibration time can be further simplified with respect to this practical set up to:

$$Optimised(TotalCalibrationTime) \approx NoOfExp \text{ (minutes)} \tag{8.1}$$

	POPT (s)	PulseCal (s)	Proposed Method (s)
No of experiments required	Up to 20	1	4
Run time per experiment	∼1-3min	∼1min	∼1min
Additional time	Human observation and cognition	N/A	Processing (0.015s)
Total (Expected)	Up to 30min	∼1min	∼4min

Table 8.3: Efficiency comparison

Table 8.3 compares the relative efficiency of each method. Successfully, the proposed method is magnitudes more efficient than the current POPT method. However, as expected, it is still significantly slower than the PulseCal method which uses a fundamentally different process. Assessing the efficiency individually, the proposed method still only takes about 4 minutes to complete, a length of time that Dr. Thomas and Dr. Hook both agree would definitely be acceptable and worth the potential increase in accuracy.

8.3   Summary

To summarise the results, it can be concluded that the proposed pulse calibration method has successfully achieved a high calibre of accuracy while drastically increasing efficiency over the current POPT method. The efficiency is still well below that of the PulseCal method, however, it can still be considered competitively as it addresses the main concern of degrading accuracy over the active lifespan of an NMR machine. Due to its base founded upon the POPT method, it is independent of linear amplifiers and their induced errors, and can remain to be accurate over time requiring less maintenance. This accuracy to efficiency optimisation makes the new method far more suitable for advanced experiments in which accuracy cannot be compromised. By optimising and fixing the relevant parameters, this method can also be made to be automatic, eliminating human input and further increasing efficiency.

Chapter 9

Conclusion

In this thesis proposal report, the structure of a new and improved $90°$ 1H pulse calibration method for NMR experiments is built. This method is hoped to prove far more suitable for advanced NMR experiments in which accuracy is paramount. The proposed solution estimates the frequency of a real sinusoid with additive white Gaussian noise and eliminates destructive effects of spin physics and human errors. This method bases itself on the current POPT method in use and use a novel frequency estimation algorithm presented by Aboutanios, Kocherry and Ye. Simulated results show great performance with the RMSE following closely to the CRLB with sufficient iterations and optimised parameters. Comparing with the existing calibration methods, the proposed method provides improved accuracy, complete automation, customisation, and optimisation with respect to a posteriori knowledge.

9.1 Future Work

The final proposed aim has been revised to a more suitable goal for the timeframe of the thesis project. However, for future work, it can be worth considering extending the automated process. With the permission of the UNSW NMR facility, the simulated code can be converted into a compatible script that can be integrated into the Bruker Topspin NMR software to test in real world applications. Topspin includes a c code compiler kit which can be investigated further if the new method is to be integrated.

To research further improvement and optimisation of this proposed calibration method, advanced experiment parameters in Topspin and specific NMR machines can be investigated and their effects compared. This thesis has only dealt with basic setup parameters in Topspin and a generalised process to run with fixed parameters for an overall average increase in accuracy. Certainly, the inclusion of dynamic parameters to adapt to different practical conditions could see to a refined and improved method.

References

[1] J. Schwinger, "On quantum-electrodynamics and the magnetic moment of the electron," *Phys. Rev.*, vol. 73, pp. 416–417, Feb 1948. [Online]. Available: http://link.aps.org/doi/10.1103/PhysRev.73.416

[2] V. Kuperman, *Magnetic resonance imaging: physical principles and applications.* Academic Press, 2000.

[3] M. Levitt, *Spin Dynamics: Basics of Nuclear Magnetic Resonance.* Wiley, 2001. [Online]. Available: https://books.google.com.au/books?id=7cAlfkJjsF0C

[4] A. D. Bain, "Radiofrequency pulses: response of nuclear spins," *eMagRes*, 2002.

[5] J. Lindon and A. Ferrige, "Digitisation and data processing in fourier transform nmr," *Progress in Nuclear Magnetic Resonance Spectroscopy*, vol. 14, no. 1, pp. 27 – 66, 1980. [Online]. Available: http://www.sciencedirect.com/science/article/pii/0079656580800021

[6] J. Keeler, *Understanding NMR spectroscopy.* John Wiley & Sons, 2011.

[7] J. C. Edwards, "Principles of nmr," *Process NMR Associates LLC, 87A Sand Pit Rd, Danbury CT*, vol. 6810, 2009.

[8] J. R. Wesener and H. Günther, "Steady state pulse calibration," *Journal of Magnetic Resonance (1969)*, vol. 62, no. 1, pp. 158 – 162, 1985. [Online]. Available: http://www.sciencedirect.com/science/article/pii/0022236485903105

[9] P. A. Keifer, "90 pulse width calibrations: How to read a pulse width array," *Concepts in Magnetic Resonance*, vol. 11, no. 3, pp. 165–180, 1999. [Online]. Available: http://dx.doi.org/10.1002/(SICI)1099-0534(1999)11:3<165::AID-CMR4>3.0.CO;2-D

[10] C. Griesinger, G. Otting, K. Wuethrich, and R. Ernst, "Clean TOCSY for proton spin system identification in macromolecules," *Journal of the American Chemical Society*, vol. 110, no. 23, pp. 7870–7872, 1988. [Online]. Available: http://dx.doi.org/10.1021/ja00231a044

[11] E. Aboutanios and B. Mulgrew, "Iterative frequency estimation by interpolation on fourier coefficients," *IEEE Transactions on Signal Processing*, vol. 53, no. 4, pp. 1237–1242, April 2005.

[12] S. Ye, D. L. Kocherry, and E. Aboutanios, "A novel algorithm for the estimation of the parameters of a real sinusoid in noise," in *Signal Processing Conference (EUSIPCO), 2015 23rd European*, Aug 2015, pp. 2271–2275.

[13] K. Mehr, B. John, D. Russell, and D. Avizonis, "Electronic referencing techniques for quantitative nmr: Pitfalls and how to avoid them using amplitude-corrected referencing through signal injection," *Analytical Chemistry*, vol. 80, no. 21, pp. 8320–8323, 2008, pMID: 18844373. [Online]. Available: http://dx.doi.org/10.1021/ac800865c

[14] I. V. Mastikhin, "Rapid determination of the {RF} pulse flip angle and spin–lattice relaxation time for materials imaging," *Journal of Magnetic Resonance*, vol. 172, no. 2, pp. 231 – 237, 2005. [Online]. Available: http://www.sciencedirect.com/science/article/pii/S1090780704003520

[15] X.-a. Mao and C.-h. Ye, "Line shapes of strongly radiation-damped nuclear magnetic resonance signals," *The Journal of chemical physics*, vol. 99, no. 10, pp. 7455–7462, 1993.

[16] P. S. Wu and G. Otting, "Rapid pulse length determination in high-resolution {NMR}," *Journal of Magnetic Resonance*, vol. 176, no. 1, pp. 115 – 119, 2005. [Online]. Available: http://www.sciencedirect.com/science/article/pii/S1090780705001837

[17] J. P. Jesson, P. Meakin, and G. Kneissel, "Homonuclear decoupling and peak elimination in fourier transform nuclear magnetic resonance," *Journal of the American Chemical Society*, vol. 95, no. 2, pp. 618–620, 1973. [Online]. Available: http://dx.doi.org/10.1021/ja00783a068

[18] J. Dohl, S. Krone, and G. Fettweis, "On the impact of non-linear amplifiers in single-carrier systems: An analytical approach," in *Vehicular Technology Conference (VTC 2010-Spring), 2010 IEEE 71st*, May 2010, pp. 1–5.

[19] E. Aboutanios, "A modified dichotomous search frequency estimator," *IEEE Signal Processing Letters*, vol. 11, no. 2, pp. 186–188, Feb 2004.

[20] D. Belega, D. Dallet, and D. Slepicka, "Accurate amplitude estimation of harmonic components of incoherently sampled signals in the frequency domain," *IEEE Transactions on Instrumentation and Measurement*, vol. 59, no. 5, pp. 1158–1166, May 2010.

[21] Y.-X. Yao and S. M. Pandit, "Cramer-rao lower bounds for a damped sinusoidal process," *IEEE Transactions on Signal Processing*, vol. 43, no. 4, pp. 878–885, Apr 1995.

[22] D. Rife and R. Boorstyn, "Single tone parameter estimation from discrete-time observations," *IEEE Transactions on Information Theory*, vol. 20, no. 5, pp. 591–598, Sep 1974.

[23] D. Moskau, "Application of real time digital filters in nmr spectroscopy," *Concepts in Magnetic Resonance*, vol. 15, no. 2, pp. 164–176, 2002. [Online]. Available: http://dx.doi.org/10.1002/cmr.10031

[24] F. J. Harris, "On the use of windows for harmonic analysis with the discrete fourier transform," *Proceedings of the IEEE*, vol. 66, no. 1, pp. 51–83, Jan 1978.

[25] Mathuranathan. (2011) Fft and spectral leakage. [Online]. Available: http://www.gaussianwaves.com/2011/01/fft-and-spectral-leakage-2/

[26] S. Ye and E. Aboutanios, "Efficient peak extraction of proton nmr spectroscopy using lineshape adaptation," in *2014 IEEE International Conference on Acoustics, Speech and Signal Processing (ICASSP)*, May 2014, pp. 5661–5665.

Appendicies

1 Risk Assessment Form

HS017

HS Risk management form

For additional information refer to HS329 Risk Management Procedure

Faculty/Division:	Elecirical Engineering		School/Unit:	University of New South Wales	
Document number	Initial Issue date 2/6/16	Current version 1	Current Version Issue date 2/6/16		Next review date

Risk management name | Thesis A Project

Form completed by	Jeffrey Siang	Signature		Date 2/6/16
Responsible supervisor/ authorising officer	ELVIS ABSOUTANVIS	Signature		Date 2/6/16

Identify the activity and the location of the activity

Description of activity	NMR Experiments

Description of location	UNSW Mark Wainwright NMR Facility

Identify who may be at risk from the activity:

This may include fellow workers, visitors, contractors and the public. The types of people affect the risk controls needed and the location may affect the number of people at risk

Persons at risk	Experiment conductors, fellow worko observers and visitors.
How they were consulted on the risk	Completing the NMR facility OHS induction

List legislation, standards, codes of practice, manufacturer's guidance etc used to determine control measures necessary

Work Health and Safety Act 2011
Work Health and Safety Regulation 2011

Identify hazards and control the risks.

1. An activity may be divided into tasks. For each task identify the hazards and associated risks. Also list the possible scenarios which could sooner or later cause harm.
2. Determine controls necessary based on legislation, codes of practice, Australian standards, manufacturer's instructions etc.
3. List existing risk controls and any additional controls that need to be implemented
4. Rate the risk once all controls are in place using the matrix in HS329 Risk Management Procedure

SHADED GREY AREAS
If you need to determine whether it's reasonably practicable to implement a control, based on the risk complete the shaded grey columns

Feel free to resize the boxes to suit your situation/the amount of text you need to use

Task/ Scenario	Hazard	Associated harm	Existing controls	Any additional controls required?	Risk Rating			Cost of controls (in terms of time, effort, money)	Is this reasonably practicable Y/N
					C	L	R		
NMR Quench	Release of Cryogens	- Skin Burn - suffocation	• Emergency exits.	No	4	D	M		
Metal objects within danger zone and devices	Disruption and magnetisation of devices such as pacemakers	- Bodily harm - Disruption of devices	• Red chains and indicators for dangerous area.	No	3	E	M		

List emergency procedures and controls
List emergency controls for how to deal with fires, spills or exposure to hazardous substances and/or emergency shutdown procedures

Fire blankets; extinguishers; Emergency exits; First aid box; Broken glass bin; Telephone
Emergency procedure clip chart.

Implementation

Additional control measures needed:	Resources required	Responsible person	Date of implementation

REVIEW

Scheduled review date:			
Are all control measures in place?			
Are controls eliminating or minimising the risk?			
Are there any new problems with the risk?			
Review by: (name)			
Review date:			

Acknowledgement of Understanding

All persons performing these tasks must sign that they have read and understood the risk management (as described in HS329 Risk Management Procedure).

Note: for activities which are low risk or include a large group of people (e.g. open days, BBQ's, student classes etc), only the persons undertaking the key activities need to sign below. For all others involved in such activities, the information can be covered by other methods including for example a safety briefing, induction, and/or safety information sheet (ensure the method of communicating this information is specified here).

Risk management name and version number:

I have read and understand this risk management form

Name	Signature	Date
ELIAS ABUJANOS	Olio Jackson	2/6/16
DONALD THOMAS	Donald CO13	2/6/16

49

2 Matlab Code

2.1 POPT Simulation

% BEGIN %

```matlab
fs = 1000; % Sampling freq
d = 1; % Total collecting duration
N = fs*d; % Number of samples
t = linspace(0,d,N); % Time vector
w = linspace(-1,1,N); % Freq scale normalised

n = 2; % Number of spectral lines
A = [1 2]; % Amplitude
f = [50 70]; % Frequency of line
T2 = [0.1 0.05]; % T2 relaxation time

eta = 1./T2; % Decay rate
p = zeros(n,N); % Individual lines (partials)
s = zeros(1,N);

fc = 45000; % Frequency of estimated sin <- Variable to be found, pw90 = 1/4fc
noOfExp = 20; % Number of One Pulse Experiments
pwInc = 5; % Each incremental pw jump
tau = linspace(0, noOfExp*pwInc, noOfExp); % PW scale
Atau = zeros(n, noOfExp); % Sinusoid
Atau2 = sin(2*pi*fc.*tau); % Simulated sin amplitude factor

% Simulate final sinusoid
for i = 1:n
    Atau(i,:) = A(i)*sin(2*pi*fc.*tau);
    figure(1);
    subplot(n,1,i);
    plot(tau, Atau(i,:));
    str = sprintf('Correlated_Peak_%d_Sine',i);
    ylabel(str);
    xlabel('Pulse_width_(\tau)');
end
```

```matlab
% Show each spectral line component
for i = 1:n
    p(i,:) = A(i)*exp(-eta(i)*t).*exp(1i*2*pi.*f(i)*t);
    figure(2);
    subplot(n,1,i);
    plot(t,real(p(i,:)));
    str = sprintf('|p_%d_(t)|',i);
    ylabel(str);
    xlabel('Time_(s)');
    s = s + p(i,:); % Create summed FID
end


% Plot FID
figure(3);
subplot(2,1,1);
plot(t,real(s));
ylabel('|s(t)|');
xlabel('Time_(s)');
title('FID');


% Plot frequency spectrum
S = fftshift(fft(s,N)); % Compute DFT of FID
S = abs(S/N); % Magnitude
subplot(2,1,2);
plot(w,S);
ylabel('|S(\omega)|');
xlabel('Frequency_(\omega/\pi)');
title('Spectrum');


% Create array spectrum
R = zeros(noOfExp, N); % Array spectrum matrix for 3D plot
R2 = 0; % Array spectrum vector for 2D plot


% Append Spectra
for i = 1:noOfExp
    R(i,:) = Atau2(i)*S(1,:); % Add each spectra as a new row in matrix
    R2 = [R2 R(i,:)]; % Append each spectra on to end of vector
end
```

```matlab
% Plot 2D Array spectrum
figure(4);
plot(R2);
ylabel('|R(k)|');
xlabel('Sample (k)');
title('2D Array Spectrum');

% Plot 3D Array spectrum
figure(5);
mesh(w, tau, R);
xlabel('Frequency (\omega/\pi)');
ylabel('Pulse width (\tau)');
zlabel('|R_k(\tau)|');
title('3D Array Spectrum');

% END %
```

2.2 Pulse Width Calibration Algorithm

% BEGIN %

```
close all;
clear all;

%% Import data from TopSpin

x = importtxt('data.txt');
pwinc = 15;
fs = 1/pwinc;

figure(1);
plot((0:length(x)-1)*pwinc,x/max(x));
xlabel('Pulse_Width_(us)');
ylabel('Normalised_Peaks');

%% pw90 estimation

rn = 25; % Internal iterations

[est,m] = AandM_est_real(x,rn);

f_est = est(1)*fs;

pw90 = 1/(4*f_est)
```

% END %

2.3 Monte Carlo Algorithm

% BEGIN %

close all ;
clear all ;

%% Monte Carlo RMSE vs SNR

% SNR range
SNRdB_L = −10;
SNRdB_H = 80;
SNRdB_Inc = 5;

SNRdB = **linspace** (SNRdB_L, SNRdB_H, 20);
RMSE = **zeros** (1, **length** (SNRdB));

% pw90 range
pw90_L = 5;
pw90_H = 20;

pw90_act = **linspace** (pw90_L, pw90_H, runs);

% Other inputs
runs = 1000;
pw_Min = 5;
pw_Inc = 5;
noOfExp = 4;

for k = 1: **length** (SNRdB)

    SE = 0; *% Initialise squared error*
    total = **length** (pw90_act);

    for n = 1: **length** (pw90_act)
        f_act = 1/(4*pw90_act(n)); *% Get frequency from pw90*
        fs = 1/pw_Inc;
        time = noOfExp/fs;
        t = **linspace** (0, time, noOfExp+1); *% pw tau vector*

```matlab
            test = sin(2*pi*f_act.*t); % Generate sinusoid

            x = awgn(test,SNRdB(k)); % Add white Gaussian noise

            rn = 25; % Internal iterations

            % Estimate frequency
            [est,m] = AandM_est_real(x,rn);
            if est ~= 0
                f_est = est(1)*fs;
                pw90_est = 1/(4*f_est);
                SE = SE + (f_act - f_est)^2;
            end
        end
    % Calculate RMSE
    sqrt(SE/length(pw90_act));
    RMSE(k) = sqrt(SE/total);
end

%% Plot results

% CRLB calculation
CRLBfreq = 12./((2*pi)^2*10.^(SNRdB/20)*noOfExp*(noOfExp^2-1));

% Convert to decibels
CRLBfreqdB = 10.*log10(CRLBfreq);
RMSEdB = 10.*log10(RMSE);

figure;
plot(SNRdB, CRLBfreqdB, SNRdB, RMSEdB);
title('RMSE vs SNR');
xlabel('SNR (dB)');
ylabel('RMSE (dB)');
str = sprintf('RMSE (%d runs)', runs);
legend('CLRB', str);

% END %
```